Design and Testing of a Piezoelectric Intramedullary Nail

By

Craig Cunningham
B.S., University of Kansas, 2018
B.S., Rockhurst University, 2014

Submitted to the graduate degree program in Bioengineering and the Graduate Faculty of the University of Kansas in partial fulfillment of the requirements for the degree of Master of Science.

_____
Chairperson Dr. Elizabeth Friis

_____
Dr. Sara Wilson

_____
Dr. Carl Luchies

Date Defended: March 27, 2020

The Thesis Committee for Craig Cunningham

certifies that this is the approved version of the following thesis:

Design and Testing of a Piezoelectric Intramedullary Nail

_____

Chairperson Dr. Elizabeth Friis

Date Approved: 03/27/2020

Abstract

The Food and Drug Administration (FDA) defines non-union as a fracture that has not fully healed within 9 months and has not shown further signs of healing after 3 months [(1)]. There are three categories in which diaphyseal fractures are differentiated: Simple fractures consisting of spiral fractures, oblique fractures, and transverse fractures, wedge fractures consisting of spiral wedge, fragmented, and bending wedge, and complex fractures consisting of spiral, irregular, and segmental fractures[(2)]. Following femoral non-union diagnosis, several options are presented to the surgeon and the patient. The five most common operative treatments for femoral non-union in order of most common, to least common are: dynamization, reamed nailing after plate, exchange reamed nailing, augmentative plate fixation, and plate fixation. The current non-union treatments presented all aim to provide a fix to non-union but fail to address the preventative issue of non-union itself. It would be advantageous to develop a surgical implant that will decrease the non-union rate while keeping surgical procedures the same for surgeons.

There are several therapeutic interventions once non-union is determined all with the common downside associated with their use of not addressing non-union before a patient suffers from non-union. These products are prescribed after a patient is diagnosed with a non-union or malunion where the most effective treatment to end non-union is to treat the source of healing issues. A product that provides such a therapy must be easily implanted by surgeons, ideally having no difference in surgical procedure as that of existing products. The product must not only decrease non-union rates but should decrease the time to fusion of those who are not in the difficult-to-fuse category. The goal in development of a new IM nail is to decrease the rate of non-union while providing the same structural integrity as existing products. The designed IM

nail shows that it will hold the necessary loads associated with a femoral fracture fixation device while also providing deformation to the lead zirconate titanate (PZT) insert allowing for power production to increase bone growth.

In the development of a piezoelectric IM nail, twelve specimen were created using piezoelectric rings. Three different specimen type (compliant layer thicknesses) were created with compliant layer (CL) thicknesses of 0.0 mm (0T), 0.7 mm (1T), and 1.4 mm (2T). Each specimen was tested in different loads of 100 N, 500 N, and 1000 N with frequencies of 1 Hz, 2 Hz, 3 Hz, 5 Hz. These loads and frequencies were to act as physiological loads as seen by orthopedic implants to characterize the power production capabilities of piezoelectric rings. This study showed that by interdigitating CLs power production as well as fracture toughness increases from 0T to 1T, from 0T to 2T and from 1T to 2T. The results show a promising development in the use pf PZT as a low frequency power generator for bone healing applications.

Acknowledgements

Dr. Lisa Friis

I would like to thank Dr. Lisa Friis for the opportunity to be a part of her lab. Without her immense knowledge and undying support this project would not have been completed. She has helped me grow, not only as a scientist, but as a person and I will be forever grateful.

Dr. Carl Luchies and Dr. Sara Wilson

I would like to thank Dr. Carl Luchies and Dr. Sara Wilson for serving on my committee and instilling their wisdom throughout my undergraduate and graduate career.

My Lab Mates

I would like to thank the group of amazing people: Morghan Alters, Chris Bowen, Ryan Downing, Tori Drapel, Josh Koski, Ember Krech, Zach Pessia, Chris Tacca, and Wade Von Kleek that I had the opportunity to work with. Without all of you I would have far less laughs and graduate school, no doubt, would be far less enjoyable. I cannot wait to see where we all end up and how we all change the world.

My Family

I would like to thank my family for always supporting me throughout the long process of my education.

Bioengineering Program

I would like to thank the Bioengineering Program for providing the opportunity as well as support throughout my graduate career.

Contents

List of Figures

List of Tables

List of Equations

Chapter 1. Introduction

1.1 Motivation

Femoral and tibial shaft fractures affect 235,000 people each year [3]. Shaft fractures are typically treated using an intramedullary (IM) nail to fix the fracture as well as provide stability to the lower limb with success rates as high as 85% - 100% [4]. Failed union is defined as a fracture that has not healed after 9 months and presents no sign of healing after three months as shown by consecutive radiographs [1]. The failure rates of femoral shaft fractures increase further in those who use tobacco products and those who suffer from diabetes. Tobacco users have a 1.6 times greater risk of nonunion [5] and people with diabetes have a 6 times greater risk of nonunion [6]. Once a failed union has occurred, there are several options surgeons look towards to aid in fracture healing. Many surgeons opt for secondary surgeries such as dynamization, reamed nailing after plating, and exchange reamed nailing all with the same goal to increase rate of bone healing and to heal the nonunion [7]–[12]. However, these secondary surgeries have not shown an increase in bone healing and require the same nine month duration to determine union [13].

Surgeons may opt for bone stimulators to aid in healing. The three main bone stimulator types are Pulsed Electromagnetic Field (PEMF), Capacitive Coupling (CC), and surgically implanted direct current (DC) stimulation. DC stimulators have shown to increase the union rate among those with bone healing risk factors[14]. PEMF and CC stimulators are external and require high patient compliance. PEMF requires patients to wear the external stimulator for a minimum of four hours a day for 270 days to achieve the level of stimulation necessary for bone growth [15] and CC is designed to be worn 24 hours a day for 270 days [16]. These two adjunct therapies require patients to constantly monitor its usage as well as the battery level to deliver the necessary stimulation to the affected area. DC stimulation, however, is implanted during surgery and delivers stimulation directly to the fracture area for 24 hours a day until the battery pack dies or is removed. The DC stimulator requires a secondary surgery to remove the battery

pack that is implanted in the soft tissue near the fracture site. The Zimmer Biomet OsteoGen® Surgically Implanted Bone Growth Stimulator Stimulator delivers 20 μA of current to the fracture site [17]. Though these therapies may be effective, the need for patient compliance and secondary surgeries leaves room for improvement in bone healing, specifically in long bone fractures.

Piezoelectric materials use, specifically lead zirconate titanate (PZT), has increased in popularity due to the minimal voltage needed to power microelectromechanical systems (MEMS) and that piezoelectric materials eliminate the need for external batteries. The use of bulk PZT ceramics in orthopedic implants has several limitations. PZT alone is very brittle and would fracture easily under the loads seen in orthopedic implants and the high impedance and high voltage output make it difficult to design circuits to deliver the necessary current to fracture sites. The introduction of many smaller PZT elements wired in parallel and stacked mechanically in series showed a decrease in impedance as well as a decrease in voltage output by the PZT stacks [18]. The use of stacks as opposed to bulk PZT lead to the discovery that interdigitating a compliant layer (CL) between each PZT element increases the power production as compared to a no CL stack [19]. This discovery was found using PZT discs for use in a spinal fusion implant. This configuration, however, could not be used in an orthopedic fracture fixation device, such as an IM nail, due to the need for a guide wire to be passed through the entire nail for surgical implantation.

The use of PZT rings for power generation has not been widely studied. By implementing PZT rings instead of discs, the ability for a guidewire to be passed through the whole implant is possible. This could lead to bone stimulating fracture fixation devices without the need for an external battery pack or secondary surgeries typical with other bone stimulating devices. It is also necessary to develop an IM nail that could incorporate PZT rings in such a way to withstand the loads seen in femoral fracture fixation devices while providing the necessary stimulation to generate bone growth. This thesis focuses on the

development of a piezoelectric intramedullary nail through the characterization of PZT ring structures as well as testing of a modular IM nail.

1.2 Specific Aims

The purpose of the first study was to determine the effect of interdigitated compliant layers (CL) between lead zirconate titanate (PZT) rings on power production in physiological loading seen by an intramedullary (IM) nail. This was accomplished by studying the effect of (1) load applied (100 N, 500 N, 1000 N), (2) frequency of load applied (1 Hz, 2 Hz, 3 Hz, and 5 Hz), and (3) CL thickness. The compliant layer thicknesses chosen were a function of the thickness of the PZT rings. 0T means there is 0 times the thickness of the rings between the rings, 1T meaning there is 1 times the thickness of the rings between the rings or 0.7 mm, and 2T meaning there is 2 times the thickness of the rings between each ring or 1.4 mm. Each load-frequency-CL combination output voltage was measured across a 38-resistor resistance sweep to determine at what resistance maximum power occurred. It was hypothesized that (1) the highest load, 1000 N, would produce the highest power output from each stack, (2) the highest frequency, 5 Hz, would produce the highest power output from each stack, and (3) the 2T or 1.4 mm CL specimen would produce the highest power of those measured.

The purpose of the second study was to determine the strain at 4 points on a simulated implant in the modular IM nail each at 90° to the other. The designed modular IM nail was inserted into a SawBones™ femur model and secured with one proximal and one distal screw. The study was accomplished by applying 0, 100, 250, 500, 750, 1000, 1250, and 1500 N loads to the head of the femur and recording the strain in the epoxy specimen. This was repeated after the specimen was rotated 90° to record the opposing side strain values.

Chapter 2. Background and Literature Review

2.1 Background in femoral non-union

The Food and Drug Administration (FDA) defines non-union as a fracture that has not fully healed within 9 months and has not shown further signs of healing after 3 months [(1)]. To determine signs of healing, consecutive radiographs at one, two, and three months are taken to assess callus formation, bone trabeculae, and fracture edges. Femoral diaphyseal (shaft) fractures occur in 10-37 people per 100,000 [(20)] with different types of fractures affecting different groups of people. High energy fractures, such as those caused by motor vehicle accidents, are associated with younger adult patients whereas low energy fractures, such as those caused by a fall, are more associated with children and the elderly [(3)(2)]. There are three distinct segments of the femoral diaphysis that fracture can occur: the proximal third, the middle third, and the distal third. A proximal fracture requires an antegrade IM nail for fixation whereas a distal third fracture requires a retrograde IM nail. A middle third fracture is typically fixed with a antegrade IM nail or by discretion of the surgeon with age and knee mobility a concern with retrograde IM nailing [(21)]. There are three categories in which diaphyseal fractures are differentiated: Simple fractures consist of spiral fractures, oblique fractures, and transverse fractures, wedge fractures consist of spiral wedge, fragmented, and bending wedge, and complex fractures are spiral, irregular, and segmental fractures[(2)].

For simple, wedge, and complex fractures an IM nail is most commonly used due to its high stabilization, shortened time to mobilization, decreased rates of infection, and the ease of monitoring healing through radiographs [(4)]. Figure 1 shows a antegrade IM nail inserted in a femur with a transverse fracture. When a reamed IM nailing is used for the treatment of femoral

Figure 1. Antegrade IM nail for femoral fracture fixation

diaphyseal fracture, the union rates are reported from 85%-100% [4]. The rates of union, however, decrease as a result of the use of unreamed nails, the use of anti-inflammatory medications (NSAIDS), the use of tobacco, and diabetes [22][6][5]. Tobacco users have been shown to have ≥1.6x greater risk for non-union than those who do not use tobacco and people with diabetes have been shown to have a ≥6x greater risk for malunion [6] [5]. The increased risk of non-union among tobacco users, and those with diabetes, make it difficult to treat femoral shaft fractures properly with the healing rates needed for successful fusion. There are several treatments for non-union, but the goal should not be to increase the rates of successful non-union treatments but instead to eliminate or greatly reduce the occurrence of non-unions. By greatly reducing non-union in

the first treatment, patient and societal costs will decrease allowing people to return to normal life faster.

2.2 Current Non-Union Treatments

Following femoral non-union diagnosis, several options are presented to the surgeon and the patient. These options are to allow the best healing in the shortest period while allowing for successful fusion of the fracture site. The five most common operative treatments for femoral non-union in order of most common, to the least common are: dynamization, reamed nailing after plate, exchange reamed nailing, augmentative plate fixation, and plate fixation. Success rates of non-union treatments vary and have their limitations. The following section will describe the operative treatment, success rates, as well as limitations regarding the specific treatment

2.2.1 Dynamization

Dynamization is an approach surgeons take to increase bone healing through increased movement or compressive loads across the fracture site. In femoral non-union, dynamization is typically performed by removing the proximal or distal interlocking screws from the IM nail for the force to be transferred to the fracture. Failed dynamization was defined as the need for secondary operation to address non-union such as bone grafting, or other non-union treatment when pain was present during weight bearing[7]. Previously, dynamization was performed 2-3 months postoperatively to most IM nails though this therapeutic intervention was determined to not be necessary as interlocking nails were introduced. Non-union dynamization has been shown to be effective in 19% to 82% with variance due to timing of dynamization, post-operative weight bearing, and indications for dynamization[7],[8]. Aside from having low efficacy, dynamization can also have the negative effect of limb shortening. An attempt has been made to

combat shortening through the use of Ilizarov telescopic rods but is not widely used. The low efficacy of dynamization could be caused by minimal force transfer or minimal movement at the fracture site due to the friction between the IM nail and the medullary canal being high [8]. There is differing opinions on the efficacy of dynamization. Some surgeons state that dynamization can increase the rate of non-union and others state it decreases healing time and increases the healing rate.

2.2.2 Reamed Nailing After Plating

Reamed nailing after plating is a surgical procedure to address non-union in femurs after a bone plate had been implanted and failed to cause union. The surgical procedure is to remove the existing bone plate and inserting a reamed IM nail [9]. Plating of femoral diaphyseal fracture has been chosen over IM nailing for various reasons. Plating provides stability to all segments of highly comminuted fracture making it the treatment of choice for these types of fractures [10]. It has been reported that with highly comminuted fractures, it is difficult to determine proper alignment of segments as well as overall rotational alignment of the femur which leads to complication rates as high as 24% [11]. It is typical for shaft fractures treated with plating that lead to mal-union or non-union to be treated with a reamed IM nailing. Post plate nailing allows for bone fragment union to occur and reamed nailing allows the surgeon to address any misalignment that may have occurred in the initial healing process. Reamed nailing has a success rate as high 72%-100% [23],[24].

2.2.3 Exchange Reamed Nailing

Exchange reamed IM nailing is the removal of existing IM nail that failed to reach union, re-reaming the medullary canal to 1-3 mm larger than the original ream, and inserting a larger nail. After initial nail is removed, a guide wire is inserted through the intercondylar region through the medullary canal. The canal is then reamed to an average diameter of 2 mm larger than the existing nail, initial nail diameter is typically 9-13 mm and the reamed nail diameter is 10-17 mm[12]. The success rate of reamed nailing varies from 47-98%[5][6]. The variability of union is caused by the severity of fracture and limb shortening being a point of failure in treatment. In comminuted fractures and large fracture gaps, exchange ream nailing has relatively low success rates with significant limb shortening. However for simple fractures, exchange nailing is a reliable choice for addressing non-union. With exchange ream nailing, a second invasive operation with long healing time is required similar to the initial IM nailing procedure. This results in increased hospital stays and patients time out of work increasing the societal cost of injuries.

2.2.4 Augmentative Plate Fixation

Augmentative plate fixation is the addition of a locking bone plate across a fractured IM nail to stabilize the fracture and give more rigidity to the existing implant, typically an IM nail. Femoral nail breaks occur in 0.5% to 3.3% of all femoral diaphysis fractures treated with IM nailing[26]. After patient had persistent pain and lack of bone regeneration shown on radiographs for three consecutive months, this patient was deemed to be a non-union [27]. With non-union presented and a clear fracture of the IM nail, the typical corrective surgery is an augmentative plate fixation. Augmentative plate fixation has union rates from 70%-100% [26]–[28]. This treatments limitations are in the added implanted hardware, typically after the initial surgery

causing greater hospital costs and longer hospital stays and it does not allow for the alignment of the femur to be adjusted if malalignment is detected after union.

2.2.5 Plate Fixation

Plate fixation is the placement of a bone plate across a fracture to stabilize, and potentially add compressive loads to the bone to aid in fracture healing. Plate fixation, however, has had non-unions reported as high as 18% [29]. The internal plate fixators are implanted either in the anterolateral or lateral peripatellar locations [30]. Kregot et al. reports that the plate fixator being inserted in these locations allows the same stability while allowing for the surgery to be less invasive to other methods of insertion. However if non-union is determined, a different approach to fracture fixation must be performed to provide the optimal patient outcome. It has been noted that patients need to delay weight bearing until there is a clear union present in serial radiographs [9]. This postponement of weight bearing will not fully utilize the healing potential of compressive interlocking screws if this type of plate is used.

The current non-union treatments presented all aim to provide a fix to non-union but fail to address any preventative measures of non-union itself. It would be advantageous to develop a surgical implant that will decrease the non-union rate while keeping surgical procedures the same for surgeons.

2.3 Predicate Devices and FDA Considerations in Design

The goal in development of a new IM nail is to decrease the rate of non-union while providing the same structural integrity as existing products. One of the most important factors in developing a modular IM nail with PZT integration is providing dynamic loading needed to utilize

the PZT for power generation. This creates several challenges in development. The first being bending and torsional integrity within the modular components and the second being the wear particles created by metal-on-metal articulation from the dynamic movement. These two challenges will likely be one of the biggest barriers for the FDA to pass. In order to alleviate the difficulty for FDA regulation and to decrease the classification of this device from a class III to a class II, several predicate devices were used to guide design and development.

2.3.1 Compression Hip Screw

The first challenge addressed in development was the structural integrity, specifically the torsional resistance. When determining the best mode of torsional resistance it was best to use compression hip screws as a predicate. One of the claims of compression hip screws are that a groove is aligned with a pin in order to resist torsional loads placed on the implant [31] [32]. Stryker's compression hip screw depicts a pin used to resist the torsional loads to be 75% into the barrel and 25% into the lag screw. This idea was used in development in the IM nail with minute changes. The pin used to withstand torsion would be a square pin as opposed to a round pin used in the compression hip screw. The pin itself would be integrated into the articulating shaft and not a separate part as to decrease the number of contact surfaces and the pin will extend equally, 50% into the articulating shaft and 50% into the barrel of the turnbuckle.

2.3.2 Knee Arthrodesis

The second challenge was determining how to apply cyclic dynamic compressive loads to the PZT element while resisting the bending moment created by intramuscular forces as well as off axis loading due to the geometry of the femur. For this, Stryker's Wichita Fusion Nail (WFN) for knee arthrodesis was used as a predicate due to the bending resistance performance as well

as applying a dynamic load to create fusion across the knee joint. The WFN is a modular three piece construction consisting of a compression screw which concentrically locks the tibial and femoral components, a tibial IM nail, and a femoral IM nail [33]. It is in the compression screw component that this product can be used as a predicate. The compression screw allows the tibial and femoral IM nails to slide on a rail which allows controlled movement across the knee joint. This component must also resist the bending loads applied to it during walking. However, the WFN relies on high compressive loads across the proximal tibia and distal femur segments to help resist bending. This design was modified slightly to have the compression screw, or in the case of the IM nail the turnbuckle, encompass more of the articulating shaft to resist the bending as well as the torsional moments.

2.3.3 FDA Considerations

For this product to show significant equivalence in the eyes of the FDA the design of the IM nail must use the same materials as well as the same modes in which the materials were used. Of particular importance is the relationship between the compression hip screw and the articulating surfaces of the IM nail. Compression hip screws are typically made from a cobalt chromium (CoCr) alloy for its high tensile strength (1400-1600 MPa) and high wear resistance [34]. Other orthopedic implants are made from stainless steel alloys and titanium alloys; however these materials have their downsides. Stainless steel has desirable mechanical properties but had poor wear and corrosion resistance. Titanium alloys have similar mechanical properties as stainless steel with better biocompatibility but has low wear resistance making it a poor choice in implants with bearing surfaces such as compression hip screws and total knee replacements. Biocompatibility, mechanical properties, and corrosion resistance must be balanced to ensure

patient safety and approval for use by the FDA. This is where the previously mentioned predicate devices must be used to show substantial equivalence.

2.4 PZT Power Generation for Bone Growth Applications

2.4.1 Piezoelectricity

Piezoelectricity is the induced polarization of a material cause by the application of an external stress such as a load [35]. Figure 2 shows how a mechanical deformation causes a voltage to be produced in a piezoelectric ring structure. This piezoelectric effect has been seen in a variety of materials such as quartz, topaz, and bone. When such a material is subjected to an external load, and imbalance of charge occurs within the material resulting in the release of electrons creating the voltage production. The type of loading determines the polarity of voltage produced where a compressive load produces either a positive or negative voltage and a tensile load creates of opposite voltage of the compressive load [36].

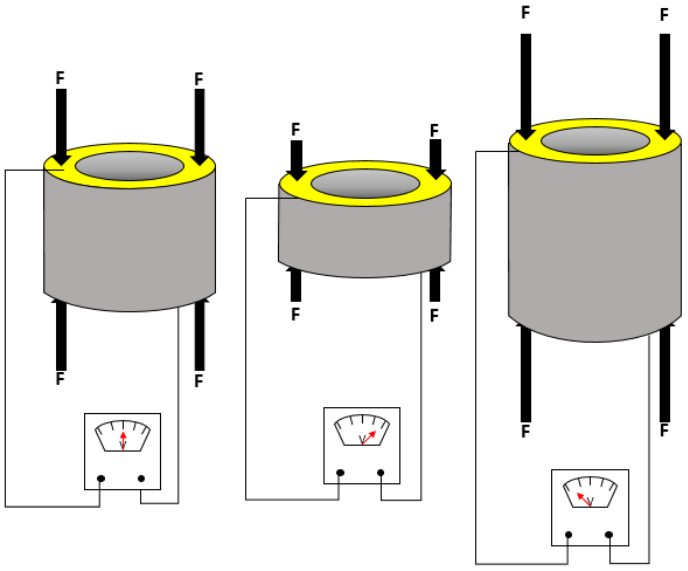

Figure 2. Piezoelectric Effect for a Monolithic Ring Structure

2.4.2 Poling Direction

The process of creating a piezoelectric ring starts from fine PZT powder. The powder is then heated to create a more uniform shape of particles. The particles are then mixed with an organic binder and shaped into the desired shape such as discs, rings, or plates. Once the particles are in the desired shape, it is then sintered creating a crystalline structure. It is critical to keep the temperature below the Curie temperature. At temperatures above the Curie temperature, PZT is a simple cubic structure with no dipole moment. This means that there will be no power production at these temperatures as there is no dipole moment creating an imbalance in charge [36]. The direction in which the imbalance in charge flows is dependent on the poling direction of the PZT. Figure 3 depicts the process of poling for PZT element. The left image is of non-poled elements. The directions of their individual dipoles are randomly oriented and if left un-poled would not create any power under cyclic loading. In order to achieve poling a strong electric field is applied on either side of the PZT element and held for a given period which causes the dipoles to align. Holding the dipoles aligned as depicted in the middle images will more permanently align the dipoles and once the electric field is removed, the dipoles may shift slightly but they will continue to be predominantly aligned with no cancelation from having opposing dipole

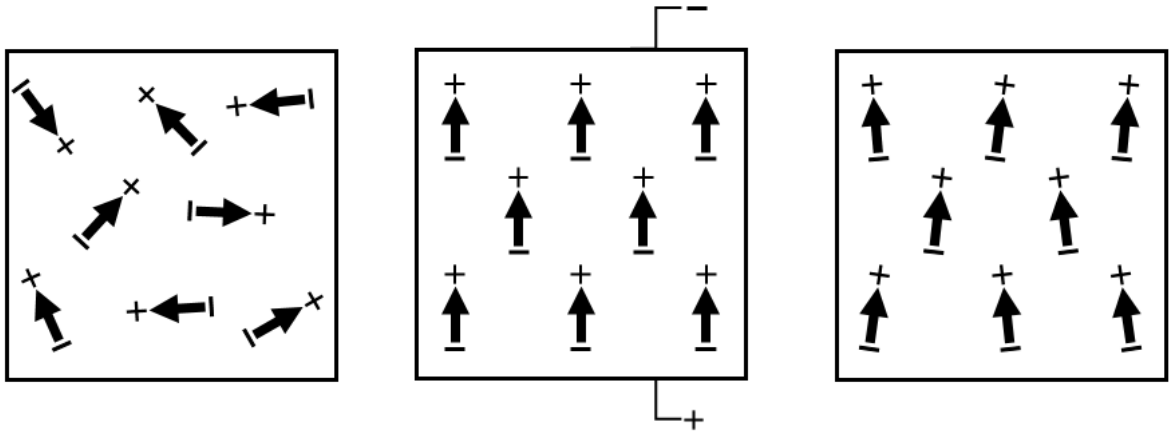

Figure 3. Poling process for PZT structures

moments. The poling direction of the PZT for application will be determined by the mode of loading. This could be utilized in application where low volume of PZT is available and high power output is necessary by increasing the efficiency of multi-layer stacked generators.

2.4.3 Applications of Piezoelectrics

There are many applications in which piezoelectric materials are advantageous. Devices such as watches, digital scales, smart phones, and ultrasound transducers are just a few applications of piezoelectrics that we use every day[26]. A more typical use is utilizing the opposite piezoelectric effect as described in 2.5.1 in that when a piezo material is subjected to an external electric field, a given deformation occurs within the material. This effect is desirable in situations where extremely precise movements must be controlled such as in the ultrasound transducers. One advantage piezoelectric materials has over others is there is no need for an external power supply to power small electronic devices. However, any load frequency that is not at resonance with the material will have a drastically lower efficiency of power generation. This poses an issue for human powered, low frequency, energy harvesting using piezoelectrics.

2.4.4 Low Frequency Power Generation of PZT Composites

The interest in low frequency energy harvesting has grown substantially in the last decade. With the further development of microelectromechanical systems (MEMS) the need for miniaturized power devices is growing. The issue with low frequency power generation, specifically with piezoelectric materials, is that loading at frequencies that differ from resonance not only decreases efficiency, but decreases the available voltage production [18]. These materials do not have uniform properties across all excitation frequencies shown by lower frequencies

having a higher source impedance. A lower source impedance means a lower resistance needed to rectify the alternating current (AC) to a direct current (DC). For bone growth applications, negative DC stimulation is needed to grow bone which poses an issue due to the high source impedance and high voltage output for low frequency power generation from PZT. Platt et al. developed a method to decrease both the source impedance and the voltage output from PZT generators. By using many thin PZT elements, connecting them mechanically in series and electrically in parallel, Platt et al. was able to decrease the resistive load that yields maximum power as compared to a monolithic stack of equal PZT volume.

The discovery to decrease source impedance in PZT generators lead to the development of composite spinal fusion implant to deliver DC stimulation to vertebrae without the use of external batteries and secondary surgeries [37]. Goetzinger et al. determined that by increasing the number of layers, wired as Platt et al. described, the source impedance and resistance in which maximum power occurs decreases. In a pilot ovine study, two sheep were implanted with macrofiber PZT spinal fusion implants to determine the efficacy of PZT as a power generator. The implants were designed to deliver 10 $\mu A/cm^2$ to the electrode [38]. The results showed that not only does PZT produce power at physiological loading, but produced grade 3 fusion as compared to the control that had grade 1 fusion at four months. However, manufacturing of a macrofiber implant was cumbersome and if commercialization of a PZT spinal fusion implant was to happen, a new manufacturing method would need to be developed. By switching from macrofibers to discs the manufacturing time and variability between specimens produced was decreased. To increase toughness of brittle PZT composites, epoxy compliant layers (CLs) were interdigitated between each disc. However, the result of interdigitating on power production was more

pronounced than the increase in toughness. By varying the CL thickness from 0.0 mm (0T), with 'T' representing the thickness of one PZT element, to 0.8 mm (2T) there was a 61% increase in power production [19]. This discovery potentially decreases the needed volume of PZT in implants while also keeping the material properties needed for orthopedic applications and could allow for self-powered bone generators to aid in non-union treatment.

2.4.5 Current Bone Stimulators for Non-union Treatment

ZIMMER BIOMET

Zimmer Biomet has a plethora of bone growth stimulators to address the issue of non-union with both invasive and noninvasive approached. They have four products in their line of Bone Healing therapies that include: EBI Bone Healing System, OrthoPak Non-invasive Bone Growth Stimulator System, SpinalPak Non-invasive Spine Fusion Stimulator System, and SpF Spinal Fusion Stimulator.

The Biomet EBI Bone Healing System is a pulsed electromagnetic field (PEMF) band that surrounds the location of the fracture. Zimmer reports healing rates upwards of 92% and provides healing 2.5 months earlier than patients with no stimulation [39] [40]. The FDA has classified this device as a Class III medical device making it a costly addition to the bone healing process. This product also needs to be worn from 3 to 10 hours a day for effective bone stimulation [16]. The usage time for this product, however effective it may be, is impractical for many users who need to go back to their normal lives as quickly as possible.

The Biomet OrthoPak® Non-invasive Bone Growth Stimulator System and SpinalPak® Non-invasive Bone Growth Stimulator System is similar to the EBI Bone Healing System in that it is an external, non-invasive therapy for the treatment of fractures and non-unions. These two

systems differ from the EBI Bone Healing System in the modality of stimulation. The OrthoPak® and Spinalpak® provide capacitive coupling stimulation that provides increased healing rates [41]. OrthoPak® and SpinalPak® provide capacitive coupling through two electrodes placed on either side of the fracture. These two therapies are designed to be worn 24 hours a day for 270 days with the user needing to change the battery pack to ensure proper stimulation throughout the whole duration [42] [43]. The constant need to ensure the battery is fully charged could decrease efficacy in the product if the patient is without a spare battery and the current battery has been depleted. Both of these Zimmer products have an FDA classification of Class III making it a costly addition to the bone healing and fusion process.

The OsteoGen™ surgically implanted bone growth stimulator is a DC stimulator used at the fracture site when patient compliance is questionable and adjunct therapy is needed to achieve union. OsteoGen™ can be used in treatment of fractures of the femur, tibia, fibula, humerus, clavicle, ulna, and radius [17]. OsteoGen differs from the other bone stimulators Zimmer Biomet offers in that the stimulation is directly at the fracture site, requires no patient compliance, and provides stimulation 24 hours a day until the battery dies or the battery pack is removed. OstenGen provides 20 µA current throughout the lifespan of the product [17]. Though this product requires little patient compliance for adequate stimulation, the implantation of a subcutaneous battery pack that will require removal leaves room for improvement. It would be advantageous of a product that delivers DC stimulation to fracture sites to require no external power source thus not requiring secondary surgeries for removal.

ORTHOFIX

CervicalStim Spinal Fusion Therapy is an external, wearable, osteogenesis stimulator use for spinal fusions in the cervical spine. The device utilizes PEMF similar to that of the EBI Bone Healing Stimulator. The device can provide 270 days of stimulation for four hours a day. The prescribed duration of treatment will be determined by the physician but will only be stimulated in four hour increments and will shut off once four hours of stimulation occur in a 24 hour period [(15)]. Orthofix provides an advantage over previously described treatments as it does not need to deliver 24 hours of stimulation during the treatment. However, the patient manual describes several adverse effects such as increased pain, numbness and tingling, headache, migraines, and nausea [(15)]. CervicalStim provided fusion in 84% of patients as opposed to 69% of control patients [(15)]. This product was assigned an FDA classification of Class III making treatment using this product much more expensive for the user.

SpinalStim Spinal Fusion Therapy is similar to that of the CervicalStim in that it provides PEMF stimulation but to the lumbar and thoracic spine. The device has the same useage as CervicalStim with the same side effects and indications. The product has a 92% rate of fusion as opposed to 65% for control for lumbar fusions [(44)].

PhysioStim Bone Healing Therapy is similar to that of CervicalStim and SpinalStim in that it provides PEMF stimulation for non-union fractures in the arm, wrist, hand, clavical, shoulder, hip, thigh, and lower ankle and foot. Orthofix does not present findings showing an increase in union rate among those who use PEMF as opposed to a control.

Zimmer Biomet and OrthoFix depict a small portion of the orthopedic bone stimulation market but their technologies cover the majority of prescribed treatments currently used.

The previously described products have a common downside associated with their use of not addressing non-union before a patient is suffering from non-union. These products are prescribed after a patient is diagnosed with a non-union or malunion where the most effective treatment to end non-union is to treat the source of healing issues. A product that provides such a therapy must be easily implanted by surgeons, ideally having no difference in surgical procedure as that of existing products. The product must not only decrease non-union rates but should decrease the time to fusion of those who are not in the difficult-to-fuse category. The product must have no external power source or no external therapies that the patient will need to undergo secondary removal therapies or be responsible for their own treatment. Finally the product must not increase the cost of care exorbitantly to ensure the needed care is accessible to the patients who need it.

2.5 Design of Piezoelectric Intramedullary Nail

2.5.1 Physiological Loads and Design Considerations

The main function of the designed IM nail is as a fracture fixation device. This means, throughout the healing process, the IM nail must resist all loads as seen by the healthy healed bone. There has been issues in determining the in-vivo forces seen by the lower limb bone structures due to inadequate simulations, difficulty in determining all variables that effects loads, and lack of empirical data to compare other approximations. An issue with these approximations is that there are multiple causes for the bone to be loaded. The main load seen is compressive load by the person directly loading their lower limbs. Tertiary loading, which

cause complexities in simulations, is torsional and bending loading cause by musculoskeletal forces and geometry for the femur specifically. Though the implant that was design was specifically for femoral fracture fixation, the design considerations, mode of primary use, and method of power production will be same for scaled down implants.

2.5.2 Loads Seen in the Femur

The complexity in loads seen by the femur has made it difficult to determine the forces needed to be resisted by an IM nail. Lu et al. at oxford conducted a study to determine the influence of muscle activity on the forces seen by the femur. The findings showed that the maximum load seen by the femur was 2715 N and corresponded to a 3.5 times greater than the subjects body weight [45]. A computational model to show loads seen by a 3-week post-operative showed similar results to the measured values presented above. The 3-week post-operative study limited the weight bearing of the leg to a maximum of 250 N. The experimental loads were found to be 5.60 Nm torsion in the Z-direction, 16.2 Nm bending moment in the anterior-posterior direction, 13.5 Nm bending moment in the medial-lateral direction, with a corresponding partial load of 300.6 N[46]. The loads presented by Schneider et al. and verified by Lu et al. were used for all design considerations of the modular segment of the piezo IM nail.

The maximum bending moment of 0.05 times BW was determined to occur at the midpoint between the top of the head of the femur to the bottom of the lateral condyle[47]. With a fracture happening at this location being the worst case for loading, the implant was designed to be located at this location. Using data presented by Lu et al. the maximum compressive load that must be resisted by the nail was 3.5 times BW and a torsional load of 0.05 times BW. Though the maximum bending moment was presented by Lu et al. it was determined that using data

presented by the ASTM standard was more appropriate as it had a higher ultimate bending moment and was more indicative of loads what would be passed by FDA. The ultimate bending moment used in design of this implant was 107.15 N-m which, using the ratios found previously, corresponds to a bodyweight of 219 kg (481 lbs) [48]. These values were used as they were what is seen by existing, FDA approved devices. In all steps in the design process FDA considerations were of the utmost importance. The goal of this work is to provide patients with a product to address nonunion before it occurs, FDA considerations are paramount to success. Without addressing FDA considerations from the beginning, the likelihood patients will benefit from this work is low. The FDA approval process will likely be the most arduous task associated with commercialization of this product.

2.5.3 Design for Manufacturability

The design process of the IM nail started with the functional structure to determine module interactions as well as part orientations within the implant. Figure 4 shows the functional structure for the IM nail. The fundamental interactions are between the implant being compressed and the piezoelectric ceramic being strained to produce current. The Incidental interactions would also be between the implant being compressed and the piezoelectric ceramic being strained. However, in this design, it is advantageous to create a design such that the fundamental and incidental interactions are the same so there are less material interfaces to create wear particles.

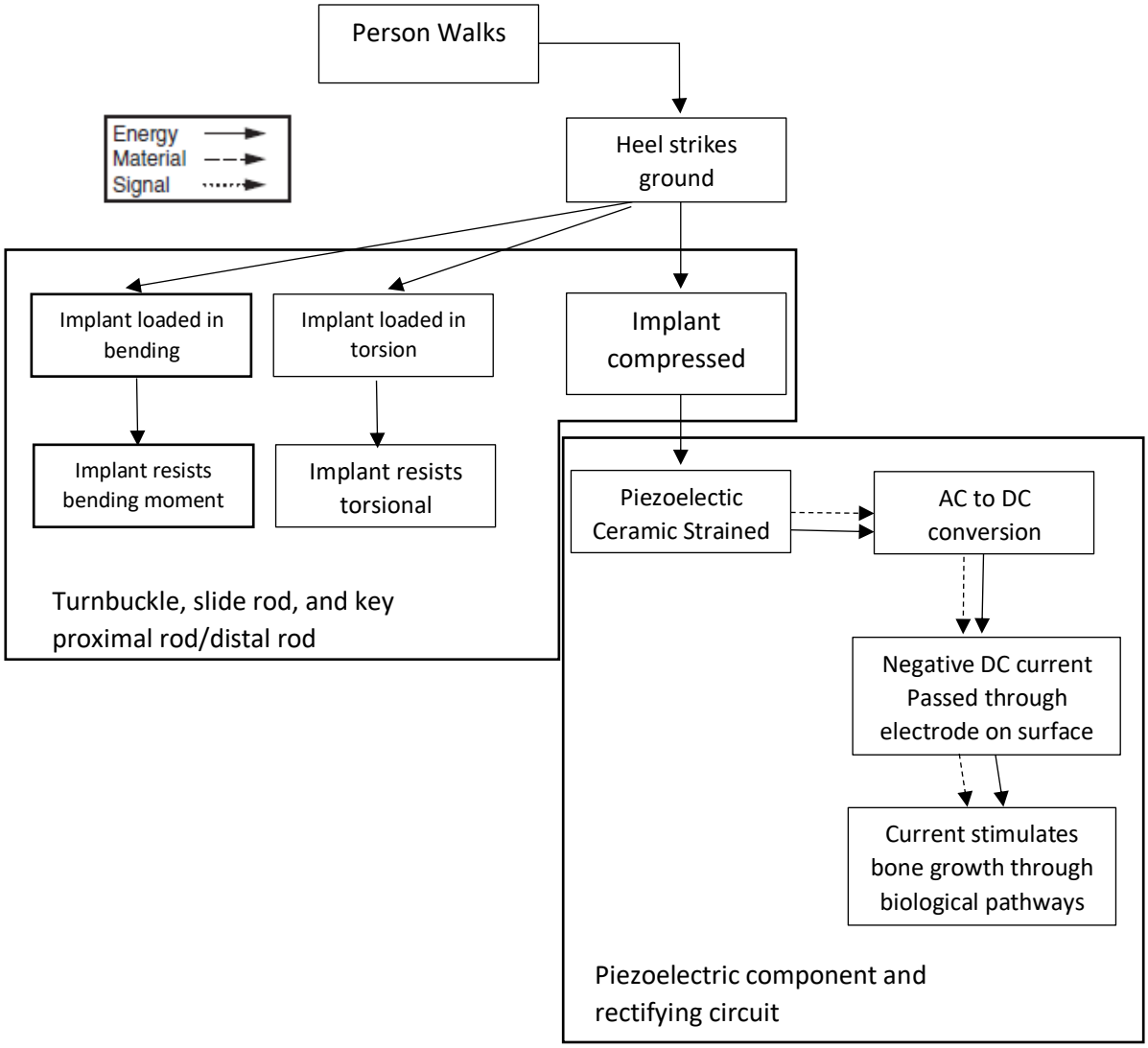

Figure 4 Functional Structure for the IM Nail

Upon initial rigid body analysis, it was discovered that an implant consisting of only PEEK, shown in Figure 5, with the piezoelectric discs inside of it would not hold the necessary bending moment or torque imposed on it using:

$$\sigma_b = \frac{My}{I} \quad (49)$$

Equation 1. Bending Moment Equation

Using the assumption that the metal-PEEK interface would transfer all bending moment to the PEEK implant and no adherence breakage happened, the maximum bending stress happens in

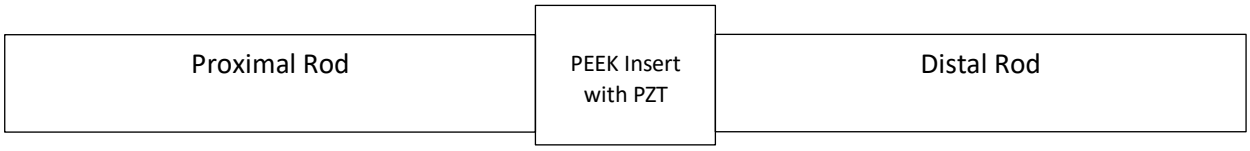

Figure 5. Initial Configuration Design for IM Nail

the tensile region thus the ultimate tensile strength of PEEK will be the limiting factor.

This led to the design of a cylindrical insert to allow for a more rigid material to pass through the inside of the implant to take the bending and torsional loads. A configuration design was determined with constraints on the outer diameter of the proximal and distal rods, the length of the slide rod, and the length of the key. Figure 6 shows the final configuration design for the IM nail. It exhibits how the piezoelectric component will surround the slide rod with a turnbuckle on one side to resist torque and disperse the load to the entire cross section of the insert.

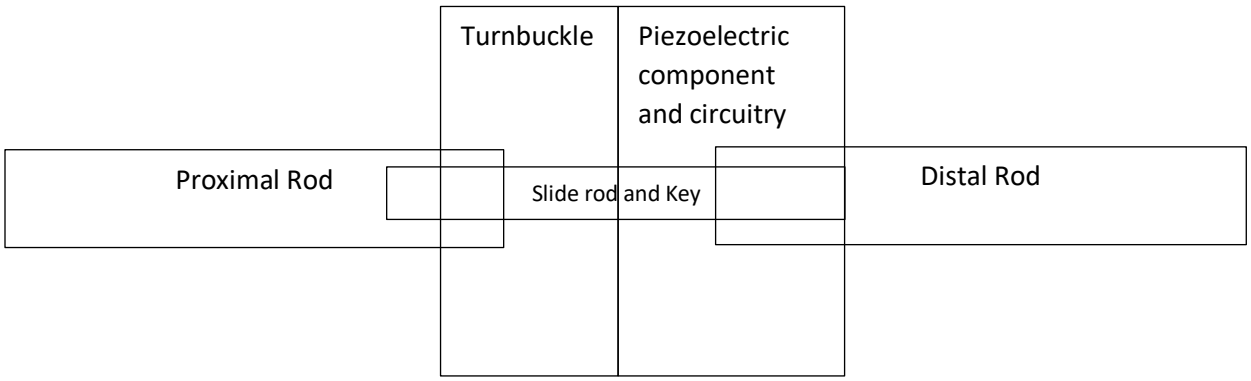

Figure 6. Final Configuration Design for IM Nail

In the configuration design, four main part interactions were defined: the proximal rod to the turnbuckle, the proximal rod to the slide rod, the piezoelectric component and the slide rod, and the slide rod to the distal rod. The slide rod and turnbuckle are key components for the success of this design. The slide rod must resist torsional and bending loads and tensile loads

when the IM nail is being removed while simultaneously fitting inside of the proximal rod. The head of the slide rods largest diameter was chosen to be 11 mm as it needed to secure the turnbuckle from sliding off the rod while remaining small enough to fit within the IM rod itself. The rods can be no larger than 16 mm OD. The threaded end inner diameter was designed to be 14 mm to allow for proper thread depth and strength of threads. The inner diameter of the cap is 5 mm as it need to be large enough to fit the guide wire surgeons use to place the IM rods. The guide wires are 3mm diameter and should fit through the 5mm through hole. Before any structural analysis could be done, materials selection would need to be completed. Existing IM nails are made of stainless steel or titanium. The stainless steel nails are less common as they have a high removal rate because wear can occur over time and release unwanted particles into the body. However titanium IM rods are becoming more prevalent due to their high corrosion resistance and sufficient mechanical properties to work as a structural body.

In the piezoelectric IM rod, neither of these materials will be sufficient for all of the parts. The turnbuckle and the slide rod will be in direct contact thus should be produced with a material of high wear resistance. The proximal and distal rods can be made of the same materials as existing rods, however, if made of different materials than the slide rod and turnbuckle, galvanic corrosion can occur. The balance of mechanical properties, corrosion resistance, and wear resistance is critical for the device to function in the body.

2.5.4 Material Choice and Failure Analysis

For the femoral component in a total knee replacement, the material of choice is a cobalt chromium alloy. Cobalt chromium alloys are known for their high corrosion resistance as well as their extraordinary wear resistance. This is the same logic used for metal-on-metal hip implants.

Thus, the material choice for the turnbuckle and the slide rod is a cobalt chromium alloy. When comparing cobalt chrome alloys to titanium alloys on the galvanic series, they exhibit similar electric potentials. Cobalt chromium varies from +0.41 to +0.42 and titanium alloys vary from +0.39 to +0.43. With the similarities in electric potentials it was determined that the proximal rod, distal rod, and connector between the slide rod and the distal rod will be produced using medical grade titanium (Ti6AL4V). The turnbuckle and the slide rod will be produced using a medical grade cobalt chromium alloy (CoCrMo). Considering the material properties for CoCrMo, the length of the cap was determined to be 36mm by using a coefficient of friction and contact pressure of μ_s=1.15 and 0.15 MPa respectively [50] using:

$$\tau = \frac{\upsilon}{A} \quad (49)$$

Equation 2. Shear Stress Equation

where τ is the ultimate shear stress approximated at 0.6UTS, υ is the shear force generated from the removal of the IM nail, and A is the cross sectional area of the cap. The shear stress was then used to find the normal force on the outer surface of the 16mm OD rod and thus the force of friction F_n to be used as maximum pullout strength. The chamfer was selected to deburr the edge on the end of the cap to eliminate sharp edges that could cause injury.

The keyway was chosen to be 3.18mm x 1.59mm x 27.5mm and was chosen to fit a 1/8" x 1/8" key. This key was calculated using key shear analysis and the minimum length of key was determined to be 10 mm using:

$$\frac{S_{sy}}{n} = \frac{F}{tL} \quad (51)$$

Equation 3. Key Length Equation

Where S_{sy} is the shear strength approximated at $0.557S_y$, n is the design factor, F is the force at

the surface of the shaft, t is the width of the key, and L is the length of the key. With a design factor of 2.5, this resulting in a key length of 25mm. Though this is only for benchtop testing. The final product will have no key but an integrated tab on the outside of the 10 mm diameter where the articulating surface is. The articulating area was chosen to be 10mm OD to provide a barrier from the head/cap to limit the movement of the turnbuckle. This decision was corroborated by performing a basic bending shear test and determining the diameter would need to be 10mm to match the bending moments reported in ASTM F1264[52] using:

$$\sigma = \frac{My}{I} \quad (49)$$

Equation 4. Bending Stress Equation

where σ is the bending stress assumed to be the UTS of cobalt chromium, M is the imposed bending moment, y is the maximum distance from the center of the nail, and I is the moment of inertia of the rod between the points of imposed moments.

ASTM F1264 depicts the ultimate bending moment and if this rod meets that standard it will prove indistinguishable from existing rods. The length of the articulating area was determined to be 27.5mm to fit the key with some extra length to allow for the circular end mill to fully encompass a 25mm length. The inner diameter of the articulating area is 5mm as it need to be large enough to fit the guide wire surgeons use to place the IM rods. The guide wires are 3mm diameter and should fit through the 5mm through hole.

The PZT area was determined to have an OD of 9mm to allow for the necessary volume of PZT to produce power in physiological conditions. This can be increased if less PZT is acceptable for power generation. The inner diameter of the PZT area is 5mm as it need to be large enough

to fit the guide wire surgeons use to place the IM rods. The guide wires are 3mm diameter and should fit through the 5mm through hole. The length of the unthreaded PZT area was arbitrarily chosen to be 6 mm to allow for a specimen of PZT volume of 287 mm^3. The threaded diameter was chosen to be 9mm to allow for the PZT section to be slid onto the implant without interference on protruding edges. The threads were chosen to be M9x1.25mm. The threads will see no load in use due to the shoulder's contact with the rod segments and will only be loaded in removal when tensile loads are applied. The length of thread was calculated to be 34mm to hold sufficient load in removal. Removal force was found using a coefficient of friction and contact pressure stated above and using equation:

$$L_t = 2d + 6 \text{ (51)}$$

Equation 5. Metric Thread Length Equation

where L_t is the length of threads and d is the nominal diameter of the threaded section in mm. The turnbuckle ID was determined to be 10mm to interface with the articulating surface and to provide necessary structure for the threads to be screwed into the IM rod. The length of thread was calculated to be 12.5mm using the same process as the threads in the PZT area. The thread diameter was chosen to be 14mm with thread specification of M14x1.5mm. This diameter and threading was chosen to allow sufficient area for the rod to be threaded and to provide the necessary surface area to transmit compressive load to the PZT implant. The length of the threads was determined to be 12.5mm using the same analysis as the PZT area threads. The stepped larger diameter was chosen to be 16mm to fit with the outer diameter of the rod being designed. This diameter cannot have any stepped variations as bone could grow into these spaces and not allow for removal if failure were to occur. It would also scrape bone from the medullary canal if

the step was in the wrong orientation thus decreasing the rigidity of the bone in that area. The unthreaded length was determined to be 17mm to allow for the 25mm key to fit within the confines of this part. This ensures no exposed parts will have contact with bone. The keyway in the turnbuckle was designed to fit with the key and keyway in the articulating surface and was chosen to be 3.18mm x 1.59mm x 29.5mm with the extra length added to fully encompass the key. The chamfer on the threaded side was chosen to be 1mm@45˚ to allow for easier threading of the part as well as decreasing sharp edges.

2.5.5 Designs

Figure 7A is what was previously described as the slide rod. For testing purposes in the lab with the machining capabilities and skills used to create this part, there is a keyway milled in

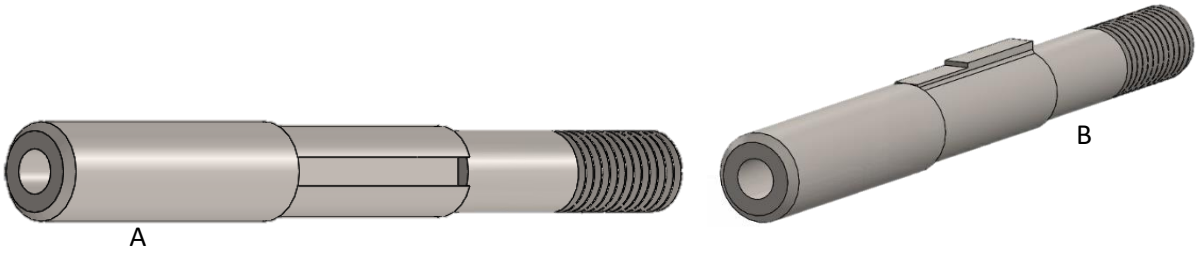

Figure 7. A) Slide Rod for Benchtop Testing B) Slide rod designed for commercial availability

the articulation area where the turnbuckle will slide to apply dynamic compression on the implant. A key will be inserted into the keyway in order to resist torsional loads. This will vary from what will be used in an actual implant. There are many stress concentrations in the keyway's interaction with the key and could likely be a source of failure. Figure 7 B depicts what the implant would look like when commercially available for use in patients. The difference between Figure 7 A and Figure 7 B is the key. It is integrated into the slide rod in the commercially available product. This will decrease the number of stress concentrations thus evenly dispersing the

torsional load throughout the whole shaft. To transfer the compressive loads from the femur to the PZT element a sliding mechanism was developed to fit around the slide rod which also holds the torsional loads from the key in Figure 7 B.

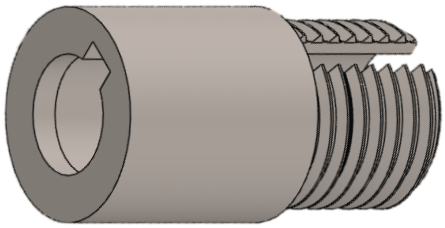

Figure 8. Turnbuckle

Figure 8 is the design for the modular turnbuckle. This component will articulate along the slide rod allowing for compressive loads to be transferred to the PZT element. This also acts as a connection point between the proximal rod and the slide rod. For this component to function properly it needs to be manufactured out of CoCr due to wear particle production. A unique aspect of this part is that the outer diameter can be changed depending on the nail sized used while still functioning as needed. This is useful in smaller femoral and tibial nails making the design useful in a range of implants. In order for this design to be a full IM nail there needed to be a single connecting piece between the slide rod and the distal rod to function as a constraint and load bearing surface for the PZT element.

Figure 9. Bottom connector

As shown in Figure 7 B there is a threaded end in which the PZT element will slide over in assembly. The threads will also be used to secure the bottom connector shown in Figure 9. The outer threads of the slide rod will fit within the inner threads of the bottom connector. The face of the bottom connector will act as the lower constraint for the PZT element and provides compressive load. Figure 10 shows the full assembly of the parts with parts 1 through 5 being: proximal rod, slide rod, turnbuckle, PZT element, bottom connector, and distal rod respectively. The order of assembly once commercially available would be to slide 3 and 4 on part 2 then securing with part 5 and applying set preload on PZT, then securing 1 and 6 for curvature alignment and fracture location. The PZT element, part 4, has a sinusoidal pattern on the outer face for the electrode to provide DC stimulation to the surrounding bone.

Figure 10. Exploded view of full modular IM nail assembly

2.5.6 Testing of Modular Implant

The goal of testing the modular implant in a physiological type loading was to initially, prove that the implant will be able to withstand loads seen in the body in addition to determine that the implant will apply compressive loads to the insert while shielding it from most of the bending loads. Knowing the material of choice for the actual implant was to be CoCr, were mechanical properties was needed to thoroughly test this implant. To determine the material that should be used in the first prototype to be tested, readily available materials were chosen to be compared to CoCr. The most likely mode of failure for this test is the bending moment caused by the off-axis load caused by the femoral diaphysis being about 10° adducted from being

vertical. The materials procured from a local vendor were 304 stainless, 1018 steel, 12L14 steel, 1045 steel, Ti 6AL4V titanium, and 4140 steel. When calculating the yield stress on the implant caused by the bending moment, it was apparent that different materials would require varying diameters of the implant area to withstand the physiological loading. Figure 11 depicts the different materials available and their respective force to yield for alternate diameters of said materials for use in the slide rod as it will hold all bending loads. It should be noted that the lines for CoCr and for 4140 steel are indistinguishable on this plot due to their similar mechanical properties. The horizontal line at 3KN is to determine, in physiological loading found by Wu et al., what diameter of each would hold this loading. The plot shows that for CoCr and 4140 steel, a diameter of 8.59 mm, is required to withstand this load. For design purses, a diameter of 10

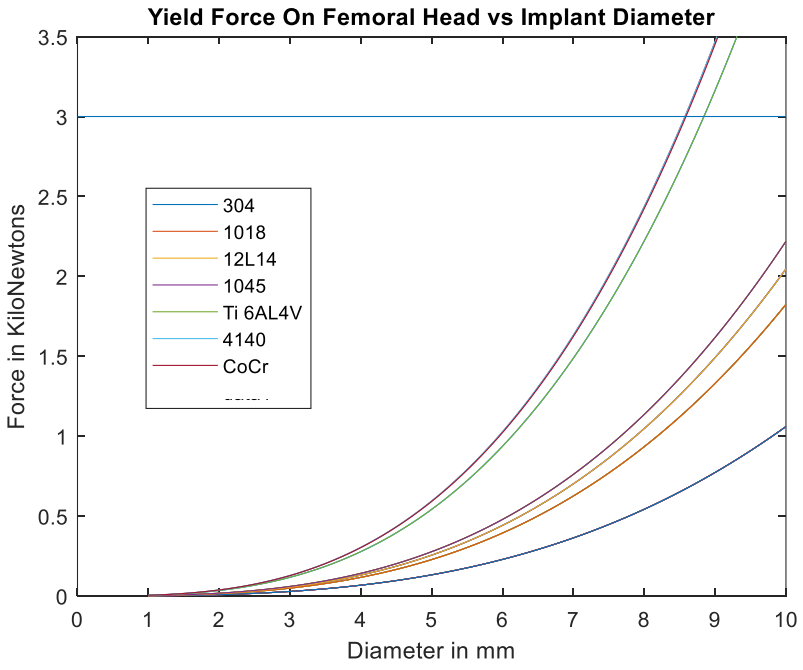

Figure 11. Different materials and their force to yield in femur configuration

mm was selected.

All parts used in testing were manufactured in the University of Kansas Machine Shop using 4140 steel. The rods to be inserted into the femur model were created with 304 stainless

from the same vendor used to acquire the bar stock to produce the slide rod, the turnbuckle, and the threaded caps. With the rods and the insert prototyped, it was inserted into the sawbones femur model that exhibits similar mechanical properties of the femur.

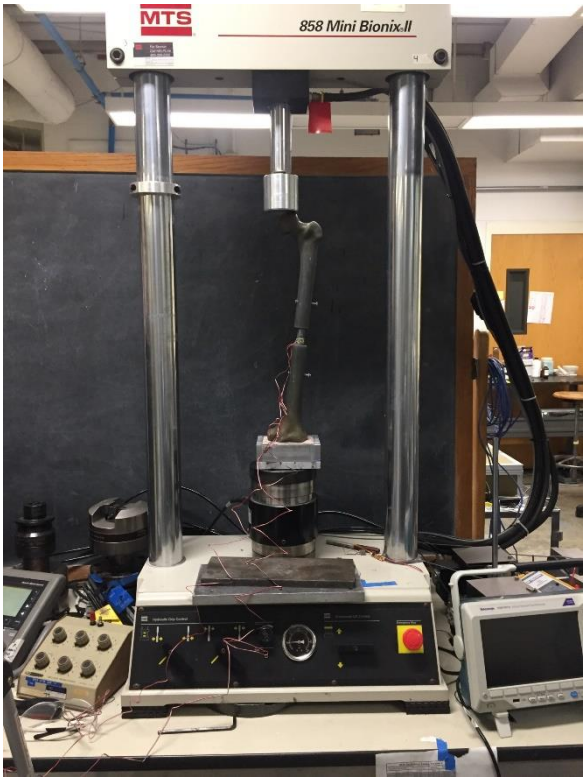

Figure 12. Testing setup for implant testing

The loads chosen to impose on the femoral head were chosen to be 100 N, 250 N, 500 N, 750 N, 1000 N, 1250 N, and 1500 N. Lower loads were initially imposed to follow the loads recorded by Schneider et al. for healing of a femur fracture with an IM nail. These loads, however, would likely not be sufficient to produce adequate power from the PZT element thus higher loads were tested. The maximum load of 1500 N was chosen to produce the bending moment applied to the implant at that high of loading. The bending moment caused by loading the femoral head to 1500 N was 30 N-m. ASTM F-1264 show bending moment yield for existing IM nails of similar

size to be 79 N-m [52]. With the goal to determine the deformation of the epoxy insert and not to determine yield of the implant, a lower load and thus a lower bending moment was chosen for this test.

2.5.7 Modular Implant Test Results

The goal of testing the modular implant with an epoxy insert including strain gauges placed at 90° angles on the insert, was to determine the strain patterns on the insert and to confirming that the implant can withstand loads seen by the body. Figure 13 shows the stress vs. strain curve for the different orientations of strain gauges. It is exhibited in the plot that the posterior and medial sides of the insert experienced the highest strains when compared to the anterior and lateral sides. This was anticipated as all of the bending moment could not be overcome by the 4140 steel implant lacking perfect rigidity. However, a compressive strain was measured across the insert, concluding, if a PZT insert was put in place of the epoxy insert, power generation is possible. The goals of the test were achieved with Figure 13 showing the strain patterns across the face of the insert and proving that the designed implant can withstand the loads imposed by physiological loading. Future testing on this implant should include ASTM

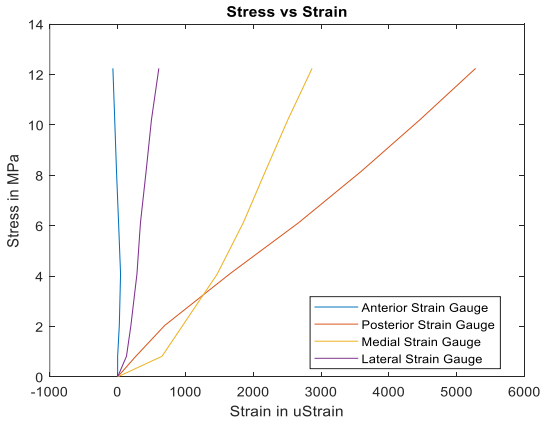

Figure 13. Stress vs Strain for Epoxy Insert on Modular Prototype

failure testing, dynamic load testing with PZT insert to determine power generation at physiologic loads, and wear particle generation testing. The designed IM nail shows that it will hold the necessary loads associated with a femoral fracture fixation device while also providing deformation to the PZT insert allowing for power production to increase bone growth.

2.6 References

1. FriJlkea JPM. Definition and classification of fracture non-unions. :4.
2. 2018, “AOOTA Classification Compendium 2018,” Journal of Orthopaedic Trauma , 32(1), pp. S33–S44
3. Antonova E, Le TK, Burge R, Mershon J. Tibia shaft fractures: costly burden of nonunions. BMC Musculoskelet Disord. 2013;14:42.
4. Toms AD, Morgan-Jones RL, Spencer-Jones R. Intramedullary femoral nailing: removing the nail improves subjective outcome. Injury. 2002;33:247–9.
5. Pearson RG, Clement RGE, Edwards KL, Scammell BE. Do smokers have greater risk of delayed and non-union after fracture, osteotomy and arthrodesis? A systematic review with meta-analysis. BMJ Open. 2016;6:e010303.
6. Gortler H, Rusyn J, Godbout C, Chahal J, Schemitsch EH, Nauth A. Diabetes and Healing Outcomes in Lower Extremity Fractures: A Systematic Review. Injury. 2018;49:177–83.
7. Vaughn J, Gotha H, Cohen E, Fantry AJ, Feller RJ, Van Meter J, Hayda R, Born CT. Nail Dynamization for Delayed Union and Nonunion in Femur and Tibia Fractures. Orthopedics. 2016;39:e1117–23.
8. Wu, C. C., 1997, “The Effect of Dynamization on Slowing the Healing of Femur Shaft Fractures after Interlocking Nailing,” J Trauma, 43(2), pp. 263–267
9. Megas P, Syggelos SA, Kontakis G, Giannakopoulos A, Skouteris G, Lambiris E, Panagiotopoulos E. Intramedullary nailing for the treatment of aseptic femoral shaft non-unions after plating failure: Effectiveness and timing. Injury. 2009;40:732–7.
10. Hakeos WM, Richards JE, Obremskey WT. Plate Fixation of Femoral Nonunions Over an Intramedullary Nail With Autogenous Bone Grafting: J Orthop Trauma. 2011;25:84–9.
11. Böstman O, Varjonen L, Majola A, Rokkanen P. The Journal of trauma: Incidence of local complications after intramedullary nailing and after plate fixation of femoral shaft fractures. J Trauma. 05/89;29:639–45.

12. Hierholzer C, Glowalla C, Herrler M, von Rüden C, Hungerer S, Bühren V, Friederichs J. Reamed intramedullary exchange nailing: treatment of choice of aseptic femoral shaft nonunion. J Orthop Surg. 2014;9:88.

13. "Femur Shaft Fractures (Broken Thighbone) - OrthoInfo - AAOS," OrthoInfo [Online]. Available: https://orthoinfo.aaos.org/en/diseases--conditions/femur-shaft-fractures-broken-thighbone. [Accessed: 08-Apr-2020].

14. Efficacy of Implanted Bone Growth Stimulation in Instrumented Lumbosacral Spinal Fusion.pdf.

15. Biomet® EBI Bone Healing System [Online]. Available: https://www.zimmerbiomet.com/medical-professionals/trauma/product/biomet-ebi-bone-healing-system.html. [Accessed: 08-Apr-2020].

17. OsteoGen Surgically Implanted Bone Growth Stimulator Surgical Technique. :24.

18. Platt SR, Farritor S, Haider H. On Low-Frequency Electric Power Generation With PZT Ceramics. IEEEASME Trans Mechatron. 2005;10:240–52.

19. Krech ED, Cadel ES, Barrett RM, Friis EA. Effect of compliant layers within piezoelectric composites on power generation providing electrical stimulation in low frequency applications. J Mech Behav Biomed Mater. 2018;88:340–5.

20. Enninghorst N, McDougall D, Evans JA, Sisak K, Balogh ZJ. Population-based epidemiology of femur shaft fractures: J Trauma Acute Care Surg. 2013;74:1516–20.

21. Yu CK, Singh VA, Mariapan S, Chong STB. Antegrade Versus Retrograde Locked Intramedullary Nailing for Femoral Fractures: Which Is Better? Eur J Trauma Emerg Surg. 2007;33:135–40.

22. Taitsman LA, Lynch JR, Agel J, Barei DP, Nork SE. Risk Factors for Femoral Nonunion After Femoral Shaft Fracture: J Trauma Inj Infect Crit Care. 2009;67:1389–92.

23. Bhandari M, Guyatt GH, Khera V, Kulkarni AV, Sprague S, Schemitsch EH. Operative Management of Lower Extremity Fractures in Patients With Head Injuries: Clin Orthop. 2003;407:187–98.

24. Wu K-J, Li S-H, Yeh K-T, Chen I-H, Lee R-P, Yu T-C, Peng C-H, Liu K-L, Yao T-K, Wang J-H, Wu W-T. The risk factors of nonunion after intramedullary nailing fixation of femur shaft fracture in middle age patients: Medicine (Baltimore). 2019;98:e16559.

25. Hak, D. J., Lee, S. S., and Goulet, J. A., 2000, "Success of Exchange Reamed Intramedullary Nailing for Femoral Shaft Nonunion or Delayed Union," Journal of Orthopaedic Trauma, 14(3), pp. 178–182.

26. Ueng SWN, Shih C-H. Augmentative Plate Fixation for the Management of Femoral Nonunion with Broken Interlocking Nail: J Trauma Inj Infect Crit Care. 1998;45:747–52.

27. Ye J, Zheng Q. Augmentative locking compression plate fixation for the management of long bone nonunion after intramedullary nailing. Arch Orthop Trauma Surg. 2012;132:937–40.

28. Lai P-J, Hsu Y-H, Chou Y-C, Yeh W-L, Ueng SWN, Yu Y-H. Augmentative antirotational plating provided a significantly higher union rate than exchanging reamed nailing in treatment for femoral shaft aseptic atrophic nonunion - retrospective cohort study. BMC Musculoskelet Disord. 2019;20:127.

29. Button G, Wolinsky P, Hak D. Failure of Less Invasive Stabilization System Plates in the Distal Femur: A Report of Four Cases. J Orthop Trauma. 2004;18:565–70.

30. Kregor PJ, Stannard J, Zlowodzki M, Cole PA, Alonso J. Distal femoral fracture fixation utilizing the Less Invasive Stabilization System (L.I.S.S.): The technique and early results. Injury. 2001;32:32–47.

31. Shaw JA. (54) LOCKING COMPRESSION HIPSCREW. :8.

32. Lower J. Zimmer_Comp_Hip_Screw_Patent.pdf. Warsaw Indiana; 1986.

33. McQueen, D. A., Wichita Fusion Nail Surgical Technique.pdf.

34. Pruitt LA, Chakravartula AM. Mechanics of biomaterials: fundamental principles for implant design. Cambridge ; New York: Cambridge University Press; 2011. 681 p.

35. Callister Jr W, Rethwisch D. Fundamentals of Materials Science and Engineering.pdf. Wiley; 2011.

36. Piezoelectric Ceramics: Principles and Applications. APC International Ltd.; 2011.

37. Goetzinger NC, Tobaben EJ, Domann JP, Arnold PM, Friis EA. Composite piezoelectric spinal fusion implant: Effects of stacked generators: COMPOSITE PIEZOELECTRIC SPINAL FUSION IMPLANT. J Biomed Mater Res B Appl Biomater. 2016;104:158–64.

38. Friis EA, Galvis SN, Arnold PM. DC Stimulation for Spinal Fusion with a Piezoelectric Composite Material Interbody Implant- An Ovine Pilot Study.pdf.

39. Murray H, Pethica B. A follow-up study of the in-practice results of pulsed electromagnetic field therapy in the management of nonunion fractures. Orthop Res Rev. 2016;Volume 8:67–72.

40. GK Frykman, Taleisnik J, Peters G, R Kaufman, Helal B, Wood V, Unsell R. Treatment of nonunited scaphoid fractures by pulsed electromagnetic field and cast. J Hand Surg Am. 1986;11:344–9.

41. Scott G, King J. A Prospective, Double-Blind Trial of electrical Capacitive Coupling in the Treatment of Non-Union of Long Bones.pdf. J Bone Joint Surg. AM; 1994.

42. Biomet ® SpinalPak® Non-invasive Spine Fusion Stimulator System Complete Manual and Package Insert. :20.

43. Biomet® OrthoPak® Non-invasive Bone Growth Stimulator System Complete Manual and Package Insert. :24.

44. Mooney V. A Randomized Double-Blind Prospective Study of the effecacy of Pulsed Electromagnetic Fields for Interbody Lumbar Fusions. Spine. 1990;15:708–12.

45. Lu T-W, Taylor SJG, O'Connor JJ, Walker PS. INFLUENCE OF MUSCLE ACTIVITY ON THE FORCES IN THE FEMUR: AN IN T/II/O STUDY. :6.

46. Schneider E, Michel MC, Genge M, Zuber K, Ganz R, Perren SM. Loads acting in an intramedullary nail during fracture healing in the human femur. J Biomech. 2001;34:849–57.

47. Duda GN, Schneider E, Chao EYS. Internal forces and moments in the femur during walking. J Biomech. 1997;30:933–41.

48. F04 Committee. Specification and Test Methods for Intramedullary Fixation Devices [Internet]. ASTM International; Available from: http://www.astm.org/cgi-bin/resolver.cgi?F1264-16

49. Hibbeler RC. Mechanics of materials. 8th ed. Boston: Prentice Hall; 2011. 862 p.

50. Gilmour LJ, Scott ML. Friction Evaluation of Orthopedic Implant Fixation Surfaces Against Bovine Bone. :1.

51. Budynas RG, Nisbett JK, Shigley JE. Shigley's mechanical engineering design. Tenth edition. New York, NY: McGraw-Hill Education; 2015. 1082 p.

52. F04 Committee. F1264.39996 Specification and Test Methods for Intramedullary Fixation Devices [Internet]. ASTM International; Available from: http://www.astm.org/cgi-bin/resolver.cgi?F1264-16

53. Memarzadeh A, Tissingh EK, Hull P, Trompeter A. Intramedullary nailing of femoral shaft fractures in adults. Orthop Trauma. 2017;31:86–92.

54. Prevalence of Long-Bone non-unions.pdf.

55. Taitsman LA, Lynch JR, Agel J, Barei DP, Nork SE. Risk Factors for Femoral Nonunion After Femoral Shaft Fracture: J Trauma Inj Infect Crit Care. 2009;67:1389–92.

56. Simonis RB, Parnell EJ, Ray PS, Peacock JL. Electrical treatment of tibial non-union: a prospective, randomised, double-blind trial. Injury. 2003;34:357–62.

57. Tobaben EJ, Goetzinger NC, Domann JP, Barrett-Gonzalez R, Arnold PM, Friis EA. Stacked macro fiber piezoelectric composite generator for a spinal fusion implant. Smart Mater Struct. 2015;24:017002.

58. Cadel E, Krech E, Arnold P, Friis E. Stacked PZT Discs Generate Necessary Power for Bone Healing through Electrical Stimulation in a Composite Spinal Fusion Implant. Bioengineering. 2018;5:90.

59. Krech ED, Cadel ES, Barrett RM, Friis EA. Effect of compliant layers within piezoelectric composites on power generation providing electrical stimulation in low frequency applications. J Mech Behav Biomed Mater. 2018;88:340–5.

60. Cease H, Derwent PF, Diehl HT, Fast J, Finley D. Measurement of mechanical properties of three epoxy adhesives at cryogenic temperatures for CCD construction. :19.

61. Inc., E. T., “EPO-TEK 301-2 Technical Data Sheet,” EPO-TEK 301-2 Technical Data SHeet [Online]. Available: http://www.epotek.com/site/administrator/components/com_products/assets/files/Style_Uploads/301-2RevXII.pdf.

60. “SpF® Spinal Fusion Stimulator,” SpF Spinal Fusion Stimulator | SpF Spinal Fusion Stimulator by Zimmer Biomet [Online]. Available: https://www.zimmerbiomet.com/medical-professionals/spine/product/spf-spinal-fusion-stimulator.html. [Accessed: 08-Apr-2020].

Chapter 3. Journal of Medical Devices Paper

This chapter is a manuscript in progress to be submitted for publication to the Journal of Medical Devices upon completion

Determination of Power Generation of PZT Rings for Use in Orthopedic Implants

Authors:

Craig Cunningham
Spine Biomechanics Laboratory,
Department of Bioengineering,
University of Kansas,
Lawrence, KS, 66045
craigc@ku.edu

Ember Krech
Spine Biomechanics Laboratory,
Department of Bioengineering,
University of Kansas,
Lawrence, KS, 66045
ekrech@ku.edu

Elizabeth Friis*
Professor,
Department of Mechanical Engineering
University of Kansas
Lawrence, KS, 66045
lfriis@ku.edu

3.1 Abstract

Tibial and femoral fractures are the most commonly fractured long bones. Intramedullary nailing is the most utilized form of fracture fixation device that results in complete healing and high fusion rates. Fusion rates decrease substantially for those who use tobacco products and those who have diabetes. Among those difficult-to-fuse populations, there are very few preventative measures to ensure fusion after a fracture. Electrical stimulation has been shown to increase the fusion rates among these populations, however, it requires multiple surgeries to remove the power source. The use of piezoelectric materials as a power source for microelectromechanical systems, that require low power, has grown substantially but are most efficient at high frequencies. The ability to develop a piezoelectric material that is more efficient at low frequencies would allow for more versatile power generation specifically in orthopedic bone healing applications. The present study determined the effect of compliant layer adaptive composite stacks on ring structures by characterizing power production at physiological loads seen in lower limb fractures. The use of compliant layers between piezoelectric rings significantly increases power production in all loading conditions. In addition, there is a theoretical increase in fracture toughness needed for the use in orthopedic implants. This study also shows how ring structures can be used in low frequency energy harvesting by increasing the power production without increasing the total volume of piezoelectric material.

3.2 Introduction

Femoral diaphyseal fractures affect 235,000 people per year with low impact fractures affecting children and the elderly populations and high energy fractures affecting younger adult populations [3][53]. Femoral diaphyseal fractures can be categorized into three groups: simple fractures, wedge fractures, and complex fractures [53]. Simple fractures consist of spiral, oblique, transverse, and subtrochanteric fractures, wedge fractures consist of spiral wedge, bending wedge, and fragmented wedge fractures, and complex fractures consist of spiral, segmental, and irregular fractures [2]. Intramedullary (IM) nailing is the most common treatment for simple, wedge, and complex fractures in adult patients due to predictable restoration, high union rate, early mobilization, and low rate of infection [4]. Non-union (i.e. failed fusion of the fracture) is relatively uncommon among femoral diaphyseal fractures when treated with a reamed intramedullary nail with success rates as high of 85-100% [54] [55]. However, the non-union rates of IM nailing is significantly increased for patients with diabetes, people who use tobacco, and those with osteoporosis [55][24]. Electrical stimulation has been shown to increase the rate of fusion in both people who use tobacco and those who do not [56]. An issue with current electrical stimulation devices is the need for an external power supply, limited device lifespan, as well as a need for a secondary surgery to remove the power supply. It would be advantageous for an implant aimed at stimulating bone growth to not need external power, and to eliminate the need to remove the power supply once union has been established.

In a pilot ovine sheep study, a macrofiber lead zirconate titanate (PZT) spinal fusion implant showed greater bone formation in the active implants as compared to the control [57]. Utilizing piezoelectrics as the power source to generate electrical stimulation within a spinal fusion implant was improved upon with the transition to piezoelectric discs as opposed to the fibers used in the ovine study implants [58]. Due to piezoelectric ceramics having poor mechanical properties for use in physiological loading conditions, compliant layer adaptive composite stacks (CLACS) were produced to increase load capabilities and fatigue resistance of PZT composite material as compared to brittle ceramics[59]. In addition to providing desired mechanical properties, CLACS also showed to increase power generation as

opposed to a cofired stack analog of PZT [59]. This increase in power generation efficiency is useful in physiological implant configurations in which direct current (DC) electrical stimulation is desired and limited space is available. The use of PZT for power generation for to provide targeted DC stimulation removes the need for an external power supply that current solutions require.

Disc configurations of PZT are useful in implant designs in which the surgical procedure does not require instrumentation to pass through the implant itself. CLACS was developed for use in spinal fusion implants however, for use in IM nailing in which a guidewire must be passed through the length of the implant, a solid disc will not suffice. A new configuration of PZT must be determined for effective bone regeneration in long bone fractures through the utilization of a piezoelectric IM nail.

The present study determined the effect of CLACS on ring structures by characterizing power production at physiological loads seen in lower limb fracture fixation devices. It was hypothesized that the implementation of CLACS will have equal or better power generation as compared to no compliant layer (CL) given constant PZT volume, size, and shape while also keeping top, bottom, inner, and outer encapsulation constant. It was expected that power generation would be consistent with results of previous studies using CLACS with PZT discs [59].

3.3 Materials and Methods

3.3.1 Materials

Modified Nave Type I PZT-4 rings were chosen for this study (SM111, STEMiNC, Doral, FL). This material was chosen due to its high elastic constant ($7.3x10^{10}$ N/m^2) and high coupling coefficient (k_p=0.58) making it appropriate for high loads seen in physiological conditions. The rings resonant mode was hoop-mode vibrational with the positive and negative electrodes on the top and bottom faces. Polarization and electrode placement were completed by the manufacturer under controlled conditions. The matrix material chosen for the compliant layers and encapsulation was EPO-TEK 301 medical grade epoxy (EPO-

TEK® 301, Epoxy Technology, Billerica, MA) for its high maximum stress of 25.86 MPa [60] and desirable volume resistivity of >2x10^{12} Ohm-cm [61] for use in piezoelectric composites.

3.3.2 Specimen Fabrication

CLACS with three different compliant layer (CL) thicknesses (n=4 per thickness) were created using PZT rings of dimensions 15 x 8.5 x 0.7 mm. Specimen were encapsulated keeping top and bottom encapsulation at 2 mm and inner and outer encapsulation at 0.5 mm. This was to be the same as diameters of typical IM nails (10-16 mm) as well as allowing for a 3 mm guidewire to pass through the center of the implant. Top and bottom encapsulation and CL thicknesses were kept consistent by creating a cylinder of pre-cured matrix material with outer diameter of 16 mm and inner diameter of 8.5 mm and cut using a low speed precision cutter (IsoMet™ Low Speed Precision Cutter, Buehler, Bluff Illinois) in 2 mm, 0.7 mm, and 1.4 mm thicknesses for top and bottom encapsulation, 1T CL, and 2T CL, respectively. 0T is defined as 0 mm layer between each ring and will be referred to as 0T, 1T CL is defined as 0.7 mm, or one PZT ring thickness and will be referred to as 1T, layer between each ring, and 2T CL is defined as 1.4 mm, or double PZT ring thickness and will be referred to as 2T, layer between each ring. Inner encapsulation was kept consistent using a pre-cured cylinder of matrix material with an outer diameter of 8.5 mm and an inner diameter of 7.5 mm and heights of 6.4, 7.8, and 9.2 mm for the different CL thicknesses.

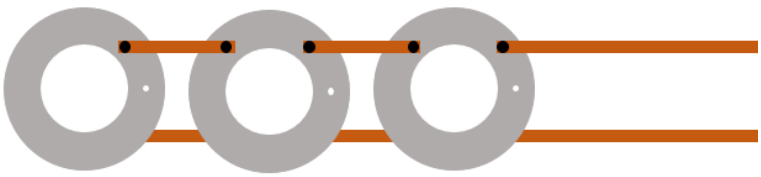

Figure 14. Wiring schematic used for wiring rings in parallel

All specimens were wired electrically in parallel using 6 individual 2 mm wide copper foil tabs shown in Figure 1. 0T, 1T, and 2T CL used four tabs of 9 mm, 10 mm, and 11 mm lengths respectively and two tabs of approximately 30 mm for all CL thicknesses. This was to ensure the center of the rings had no

obstructions and maintained concentricity when stacked to align mechanically in series. 3 rings per specimen were connected using conductive epoxy (EPO-TEK® H20E, Epoxy Technology, Billerica, MA) with each strip of copper foil. A 2 mm epoxy base was fit with the desired height, either 6.1 mm, 7.5 mm, or 8.9 mm, inner encapsulation. For the 0Tpecimen, the top face of the bottom encapsulation ring was coated with a thin layer of uncured epoxy and, with the rings folded in an accordion fashion, the rings were placed on the center post ensuring concentricity with a thin layer of epoxy between each ring to ensure adherence. The top ring was coated in a thin layer of epoxy and the top encapsulation epoxy ring was placed on top and was weighted to apply a small compressive load during curing. 1Tand 2T specimen were created in a similar way with the compliant layer being added with a layer of epoxy on top and bottom of CL ring and inserted between each ring before being placed on the center post. After a 24 hour room temperature cure, each specimen was post cured for 2 hours at 60°C. Post cured specimen were then encapsulated in epoxy with an outer diameter of 16 mm heights of 6.4, 7.8, and 9.2 mm for 0T, 1T, and 2T specimen, respectively. Post encapsulation impedance measurements were taken to ensure ring connectivity.

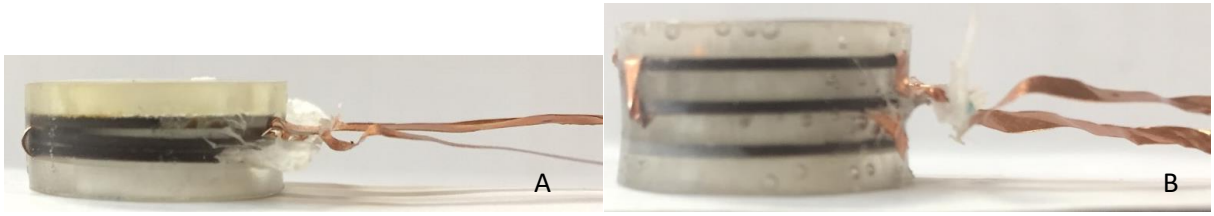

Figure 15. A) 0.0 mm compliant layer specimen, B) 1.4 mm compliant layer specimen

3.3.3 Electromechanical Testing

Each specimen was tested electromechanically to determine voltage output at varying frequencies and loads across a resistance sweep to simulate physiological loading of orthopedic implants as well as to determine optimal circuit design. The loads selected were to best characterize CLACS in a partial weight bearing IM nail. Partial weight bearing was chosen for loads due to the inability for a patient to fully load the femur after a fracture fixation procedure. A preload of 1200 N with a cyclic load of 100,

500, and 1000 N amplitude with frequencies of 1, 2, 3, and 5 Hz was applied to each specimen using an MTS MiniBionix 858 (MTS, Eden Prairie, MN). All loads and frequency output voltages were measured across a shunting resistance sweep from .25 MΩ to 602 MΩ. RMS voltage was calculated using a MATLAB (Mathworks, Natick, MA) code, $V_{RMS} = V_{out}/\sqrt{2}$, and average maximum power was calculated for each frequency and loading condition, $P = V_{RMS}^2/R$ and a two-way ANOVA with a Tukey-Kramer post-hoc analysis was used to determine differences between groups ($P<0.05$)

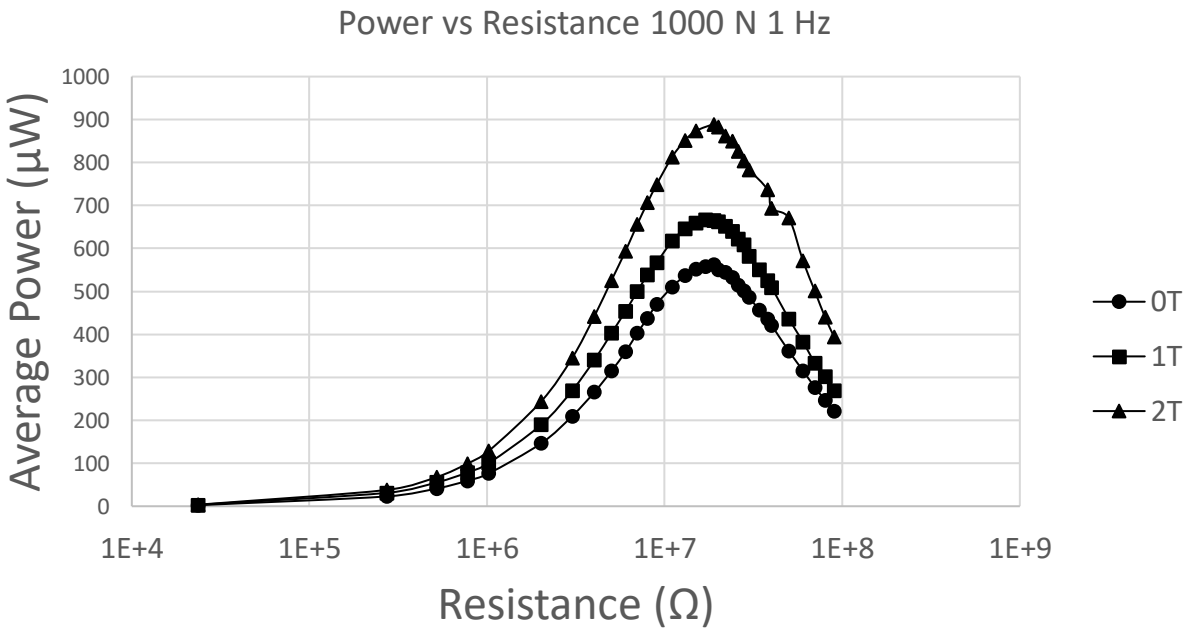

Figure 16. Average power output as a function of compliant layer thickness and resistive load for 1000 N 1 Hz

3.4 Results

3.4.1 Power Generation

The power generation of each specimen was measured across a shunting resistance sweep from 250 KΩ to 603 MΩ. Maximum power generated occurred at the 1000 N 1 Hz loading condition as shown in the average power vs. resistance plot in Figure 16. Maximum power generated for 0T, 0.7 mm, and 1.4 mm CL was 3400 µW, 3785 µW, and 4908 µW

respectively. At this loading condition, maximum power occurred at the same resistance of 3 MΩ for all groups.

Table 1 shows the effect of compliant layer on the power generated at 1000N 5 Hz which shows a significant ($p<0.05$) increase in power production from 0T to 1T, from 0T to 2T and from 1T to 2T. In this configuration and loading condition there was a 23% increase in power from 0T to 1T CL thickness, a 59% increase in power from 0.0 mm to 1.4 mm CL thickness, and a 30% increase in power from 0.7 mm to 1.4 m CL thicknesses ($p<0.05$). This relationship held true for all loading conditions ($p<0.05$).

Compliant Layer Thickness (mm)	Average Maximum Power (μW)
0.0	3088±494
0.7	3785±516
1.4	4908±925

Table 1 Average maximum power generated as a function of compliant layer thickness at 1000 N and 5 Hz

3.4.2 Frequency

The power generated at 1000 N for 1, 2, 3, and 5 Hz loading is presented in Figure 17. As anticipated, maximum power generation occurred at 5 Hz for all CL thicknesses and loads ($p<0.05$). At each loading frequency at 1000 N, 1T CL and 2T CL thicknesses produced significantly more power than the 0.0 mm CL and this held true for all other loads applied ($p<0.05$). The frequency of loading applied had a linear increase for each CL thickness as shown in Figure 19. The 2 Hz frequency doubled power production, 3 Hz tripled power production, and 5 Hz had a fivefold increase in power production when compared to the 0.0 mm CL thickness ($p<0.05$) at 1 Hz. The slope of each CL thickness held consistent with the power production with the slope of the 0.7 mm CL and the 1.4 mm CL thicknesses bring 1.45 and 1.13 times greater than that of the 0T specimen. The slop represents the amplification for each CL thickness showing that 2T CL thickness has the highest amplification as compared to 1T ($p<0.05$).

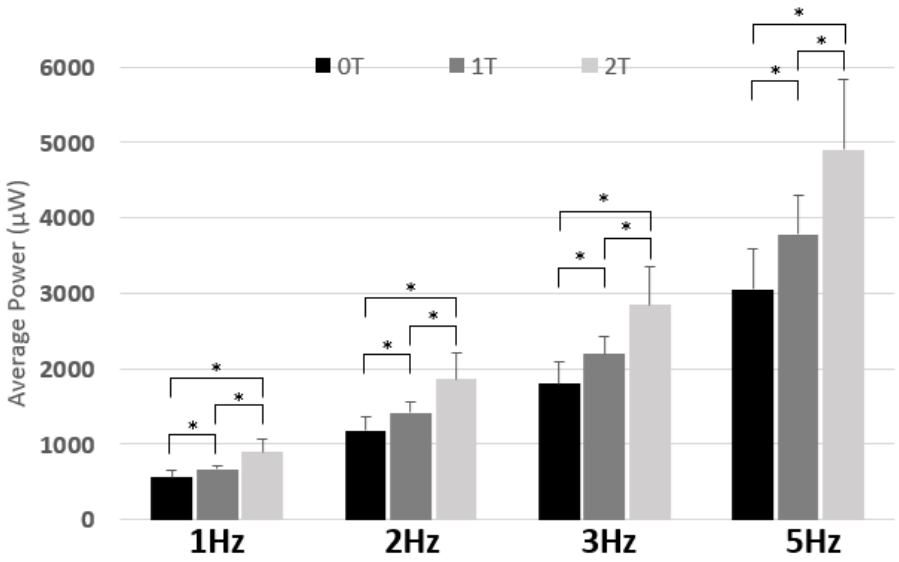

Figure 17. Power generated as a function of loading frequency for 1000 N amplitude load

3.4.3 Loading

The increase in load caused a significant increase in power production for all CL thicknesses and frequencies ($p<0.05$). Increasing load has a nonlinear result of power production with a second order polynomial being the best fit with R=1 for all CL thicknesses and frequencies as shown in Figure 19. The coefficients for each trend line follows the same increase from 0T to 1T, 0T to 2T and 1T to 2T of 1.05, 1.40, and 1.33 respectively. There was approximately a 120-fold increase in power from 100 N to 1000 N, a 27 –fold increase in power from 100 N to 500 N, and approximately a 5-foldincrease in power from 500N to 1000 N and was consistent for all frequencies ($p<0.05$).

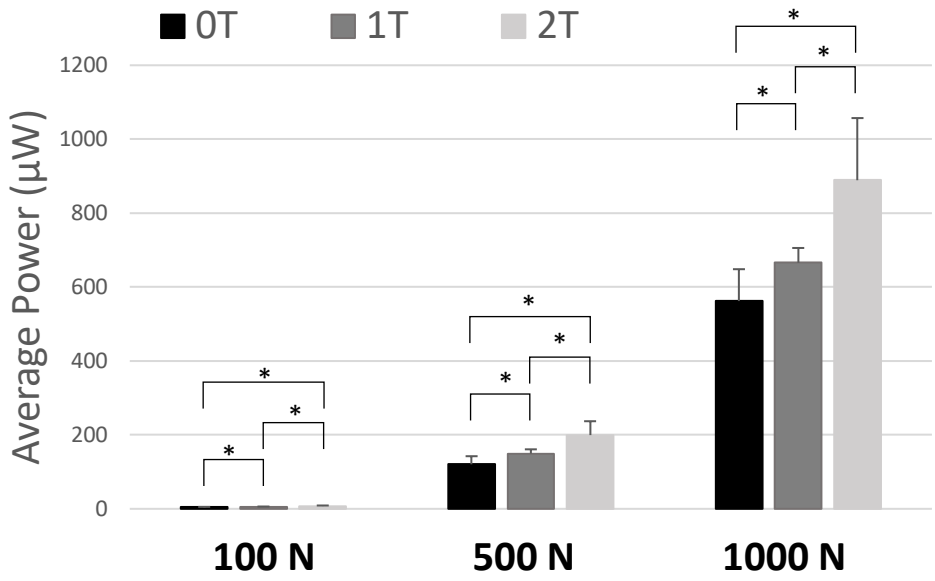

Figure 18. Average maximum power generated as a function of magnitude of applied load at 1 Hz for all compliant layer thicknesses

3.5 Discussion

The purpose of this study was to determine the effect of CLACS on ring structures by characterizing power production at physiological loads seen in lower limb fracture fixation devices. It was shown by Krech et al that interdigitating CLs between discs significantly increased power production while decreasing source impedance as compared to a monolithic stack [(59)]. It has been shown that by connecting the PZT elements electrically in parallel and mechanically in series, the resistance at which maximum power occurs and the maximum voltage produced decreases both of which are needed for medical device applications [(18)].

The results showed that maximum power occurred at 1000 N, 5 Hz, and 3 MΩ for all CL thicknesses as shown in Figure 18. Previously developed low frequency harvesting devices using PZT have shown power production of 1243 µW for Krech et al. and 566 µW for Goetzinger et al. for loading conditions of 1000 N 1 Hz [(57),(59)]. For 1000 N and 1 Hz, the 0T ring structures in this study produced 1501 µW at the same resistance of 16 MΩ. The previous comparison, however, does not accurately compare power

production at low frequencies as there is a difference in volume of PZT for the three studies and a differing resistance at which power production occurred. For comparison, power for all three studies was taken at 1000 N 1 Hz and 16 MΩ. Controlling for volume of PZT (V_{PZT}), Goetzinger and Krech's specimen generated 2.6 and 7.9 μW/mm^3 respectively whereas the ring structures produced 6.0 μW/mm^3 for the same load, frequency, and resistance using power produced by the 0T specimen. If maximum power density is calculated for rings, this results in 7.4 μW/mm^3 at 1000 N 1 Hz. Maximum power for rings occurred at 8 MΩ, much lower than that of macrofibers and discs. A lower resistance at which maximum power occurs, allows for much a much smaller circuit to rectify the AC to DC needed for bone stimulation.

A higher power density for discs shows it may be better at power amplification, however, it may not be the structure of choice for certain implants and modes of loading. In orthopedic implant design, surgical procedure for implantation as well as loading conditions must be addressed. If surgeons are required to change surgical procedures surgeon adoption and use of this product would be low. Specifically for an IM nail, a guidewire is fed through the reamed medullary canal to guide placement of the nail. The guide wires, therefore, require a completely hollow implant. In addressing long bone fracture fixation, PZT rings are more advantageous than discs or plates in implant design. The loads seen in lower limb fracture fixation devices would be much higher and at half frequency seen by the spinal fusion devices presented by Goetzinger et al. and Krech et al., but for baseline comparisons the loads and frequencies of testing were kept consistent with previous work. The maximum loads seen by the femur were reported to be 3.5 times the patient's bodyweight under normal, 1 Hz, walking frequencies [45]. However this does not accurately represent the loads an IM nail would experience during the weeks post-surgery when the patient is not fully weight bearing. By testing power production in loads ranging from 100 N to 1000 N, the power developed by different patients throughout the healing process could be determined. Power generation as a function of loading frequency had a linear relationship as shown by Figure 19. Frequency of loading also had an inverse relationship to the resistance at which maximum

power occurred. At 1000 N, that of partial weight bearing lower limb implants, maximum power occurred at 5 Hz as shown by Figure 17 however this is a much higher frequency than would be seen by any orthopedic implant. Typical spinal fusion implants would see a frequency of 2 Hz and lower limb fracture fixation devices would see a 1 Hz loading condition. For a 1000 N load, 2 Hz, 3 Hz, and 5 Hz increased the power generated by 2.1 times, 3.2 times, and 5.4 times respectively as compared to 1 Hz loading. This relationship was consistent for 0T, 1T, and 2T CL specimen.

With the use of PZT rings as the power source in a bone stimulating IM nail, the expected power that is achievable through the rectifying circuit will be less than the maximum power in physiological conditions of 889 μW at 1000 N and 1 Hz loading. Even with a decrease in power, the PZT rings can be expected to deliver enough current through a rectifying circuit to stimulate bone growth consistent with existing DC stimulators. Existing DC stimulators deliver 20 μA of current through each electrode for a total of 40 μA [62]. These currents are established to deliver 10 μA/cm^2 [38], the needed current density for bone stimulation. The current density that will be delivered using the PZT power source will be the same as existing products of 10 μA/cm^2. The current density will be a function of electrode length as well as the resistance of the rectifying circuit used to convert AC to DC. PZT rings deliver substantial power at low resistances which is useful when it comes to circuit design; at a lower resistance the circuit size will decrease making it easier to be self-contained in the implant itself. The size of the circuit can also be determined by the area of the electrode that will deliver the 10 μA/cm^2 current density. With clever design of the electrode, the necessary current density can be achieved allowing for PZT rings to be used as the power source for orthopedic implants.

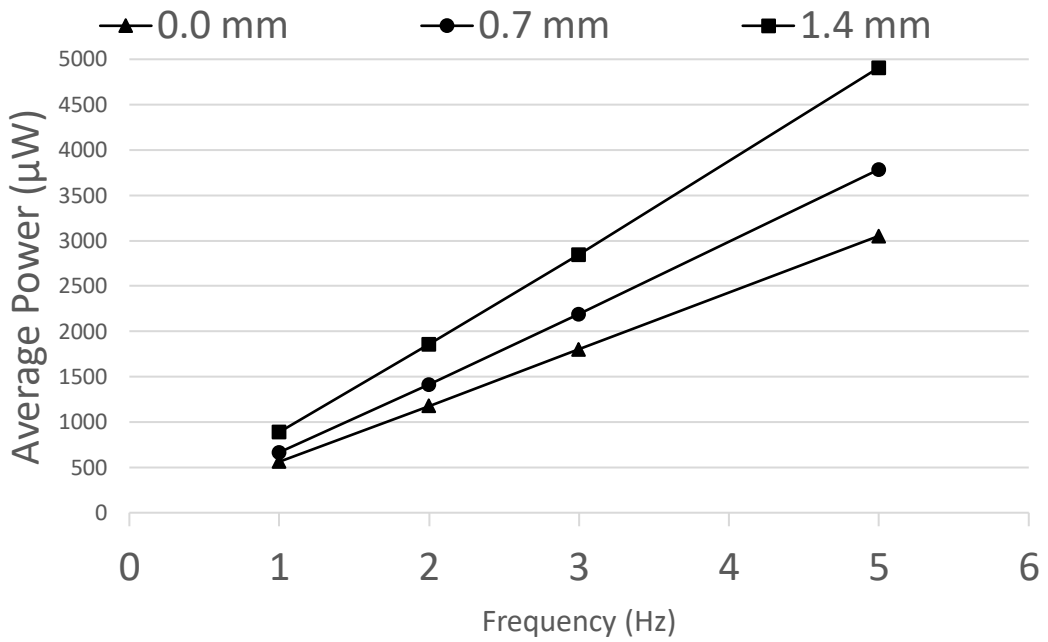

Figure 19 Depiction of linear relationship between power generated and frequency of loading at 1000 N

Future work should include testing more CL thicknesses to determine if there is an optimal CL thickness to provide the most power from this configuration of PZT. An optimal thickness of CL can aid designers in creating implants with the maximum power generation for the application. There should also be a finite element model to best represent how CLACS amplifies power and will allow designers to test designs theoretically before creating a physical product.

Moving forward, it is suggested to utilize the 2T CL for implant design with rings due to the increase in power generated and the increase in energy to fracture as both of these parameters are critical for orthopedic bone healing applications.

3.6 Conclusion

The use of compliant layers between PZT rings significantly increased power production in all loading conditions and CL thicknesses. This study also shows how ring structures can be used in low frequency energy harvesting by increasing the power production without increasing the total volume of

PZT. Existing products rely on external power sources implanted in soft tissue during initial surgery to power the bone stimulators. The use of PZT as a power generating produced substantial power at physiological conditions making PZT rings a potential power source for hollow orthopedic bone stimulators.

3.7 Acknowledgements

This work was supported by a University of Kansas Go Grant (KU Award ID 00049907). The authors would like to thank the University of Kansas for their support of graduate researchers through assistantship funding.

3.8 Conflict of Interest

None

3.9 References

[1] Antonova, E., Le, T. K., Burge, R., and Mershon, J., 2013, "Tibia Shaft Fractures: Costly Burden of Nonunions," BMC Musculoskelet Disord, **14**(1), p. 42.

[2] Memarzadeh, A., Tissingh, E. K., Hull, P., and Trompeter, A., 2017, "Intramedullary Nailing of Femoral Shaft Fractures in Adults," Orthopaedics and Trauma, **31**(2), pp. 86–92.

[3] 2018, "AOOTA Classification Compendium 2018," Journal of Orthopaedic Trauma , **32**(1), pp. S33–S44.

[4] Toms, A. D., Morgan-Jones, R. L., and Spencer-Jones, R., 2002, "Intramedullary Femoral Nailing: Removing the Nail Improves Subjective Outcome," Injury, **33**(3), pp. 247–249.

[5] Tzioupis, C., and Giannoudis, P. V., 2007, "Prevalence of long-bone non-unions," Injury, **38**.

[6] Taitsman, L. A., Lynch, J. R., Agel, J., Barei, D. P., and Nork, S. E., 2009, "Risk Factors for Femoral Nonunion After Femoral Shaft Fracture:," The Journal of Trauma: Injury, Infection, and Critical Care, **67**(6), pp. 1389–1392.

[7] Wu, K.-J., Li, S.-H., Yeh, K.-T., Chen, I.-H., Lee, R.-P., Yu, T.-C., Peng, C.-H., Liu, K.-L., Yao, T.-K., Wang, J.-H., and Wu, W.-T., 2019, "The Risk Factors of Nonunion after Intramedullary Nailing Fixation of Femur Shaft Fracture in Middle Age Patients:," Medicine, **98**(29), p. e16559.

[8] Simonis, R. B., Parnell, E. J., Ray, P. S., and Peacock, J. L., 2003, "Electrical Treatment of Tibial Non-Union: A Prospective, Randomised, Double-Blind Trial," Injury, **34**(5), pp. 357–362.

[9] Tobaben, E. J., Goetzinger, N. C., Domann, J. P., Barrett-Gonzalez, R., Arnold, P. M., and Friis, E. A., 2015, "Stacked Macro Fiber Piezoelectric Composite Generator for a Spinal Fusion Implant," Smart Materials and Structures, **24**(1), p. 017002.

[10] Cadel, E., Krech, E., Arnold, P., and Friis, E., 2018, "Stacked PZT Discs Generate Necessary Power for Bone Healing through Electrical Stimulation in a Composite Spinal Fusion Implant," Bioengineering, **5**(4), p. 90.

[11] Krech, E. D., Cadel, E. S., Barrett, R. M., and Friis, E. A., 2018, "Effect of Compliant Layers within Piezoelectric Composites on Power Generation Providing Electrical Stimulation in Low Frequency Applications," Journal of the Mechanical Behavior of Biomedical Materials, **88**, pp. 340–345.

[12] Cease, H., Derwent, P. F., Diehl, H. T., Fast, J., and Finley, D., "Measurement of Mechanical Properties of Three Epoxy Adhesives at Cryogenic Temperatures for CCD Construction," p. 19.

[13] Inc., E. T., "EPO-TEK 301-2 Technical Data Sheet," EPO-TEK 301-2 Technical Data SHeet [Online]. Available: http://www.epotek.com/site/administrator/components/com_products/assets/files/Style_Uploads/301-2RevXII.pdf.

[14] Platt, S. R., Farritor, S., and Haider, H., 2005, "On Low-Frequency Electric Power Generation With PZT Ceramics," IEEE/ASME Transactions on Mechatronics, **10**(2), pp. 240–252.

[15] Lu, T.-W., Taylor, S. J. G., O'Connor, J. J., and Walker, P. S., "INFLUENCE OF MUSCLE ACTIVITY ON THE FORCES IN THE FEMUR: AN IN T/II/O STUDY," p. 6.

[16] Robert Jones, 1984, *Mechanics of Composite Materials.Pdf*, Taylor & Francis, Inc

[17] Budynas, R. G., Nisbett, J. K., and Shigley, J. E., 2015, *Shigley's Mechanical Engineering Design*, McGraw-Hill Education, New York, NY.

Chapter 4 Conclusion and Recommendations

4.1 Conclusion

The goal of the initial study was to determine the effect of interdigitated compliant layers (CL) between lead zirconate titanate (PZT) rings on power production in physiological loading seen by an intramedullary (IM) nail. It was concluded that with an increase in frequency and load the power generated was also increased for all CL thicknesses. Frequency had a linear relationship on power whereas load applied was not a linear relationship. By increasing CL thicknesses, the power generated also increased for all load and frequency combinations.

The purpose of the second study was to determine the strain pattern on a simulated implant in the modular IM nail. It was concluded that a non-uniform strain pattern occurred on the implant likely due to the large bending moment at the location of the insert. However, compressive load was applied to the insert implying that, when loaded in cyclic dynamic loading, power could be generated if a PZT insert was fabricated. This also illustrates that a modular IM nail is possible and can withstand compressive loads seen by the IM nail during fracture healing.

4.2 Limitations

There were several limitations with the first study conducted. When fabricating the PZT specimen, there was not a 0.0 mm gap between each ring in the 0T specimen which could lead to a CL- related amplification of power. With all specimen created, the rings may have shifted slightly resulting in imperfectly parallel rings leading to off-axis loading and potential power

generation decreases. It is also worth noting there could be microscopic air bubbles created when pouring the epoxy into the molds to encapsulate the specimen which could cause variability in power generation.

There were also several limitations with the second study conducted. When aligning the femur to 10° adduction to simulate single leg stance, the angle could be slightly varied which would change the loading on the insert and ultimately impact the strain pattern on the insert. The rods inserted into the femur model were straight rods as opposed to curved rods to match the curvature of the medullary canal and could affect the loading on the insert, as well.

4.3 Future Work

Future work should include creating a PZT specimen to be tested in the modular IM nail to determine power generation in a more accurate physiological simulation. This would also require a PZT specimen to be designed to fit within the implant to prevent too large of a bending moment on the implant thus causing bending yield. The implants should be created using a medical grade CoCr alloy to most accurately test how the medical implant would be used. Finally, for future testing, the PZT implant should be designed to that decrease the impedance of the specimen as a whole thus decreasing the resistance that maximum power occurs.

Appendix A: Supplementary Figures

a) 100 N 1 Hz

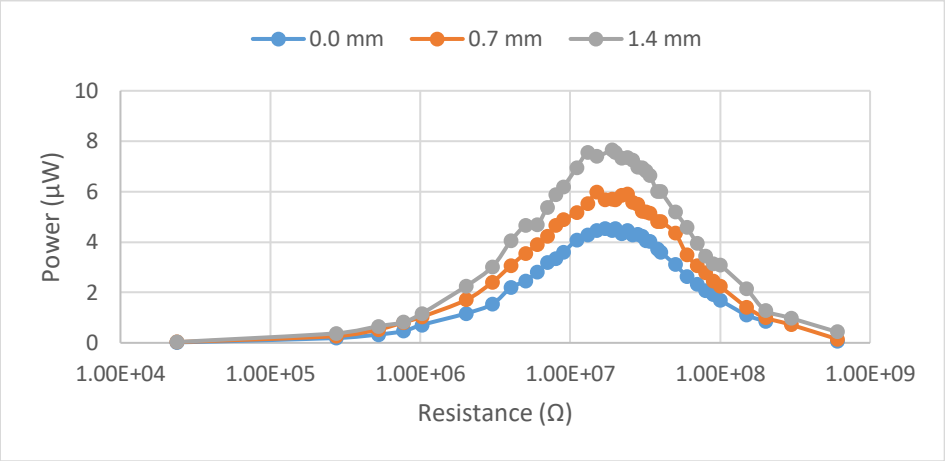

b) 100 N 2 Hz

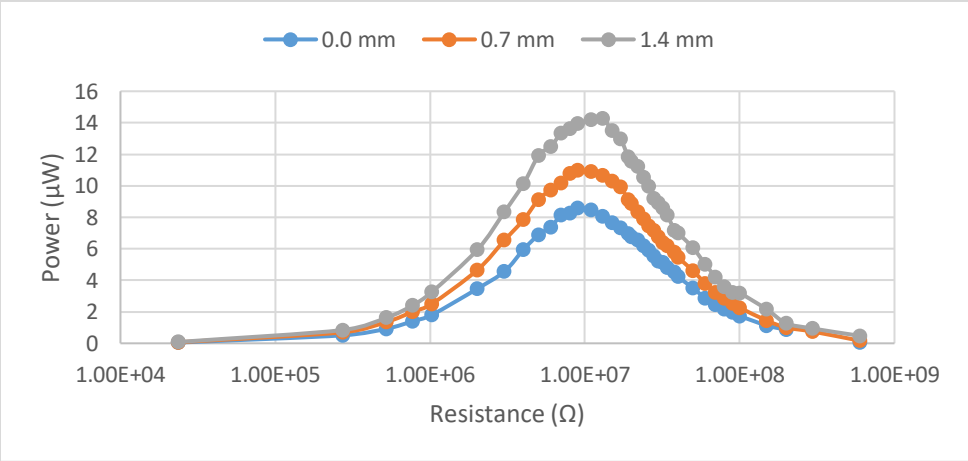

c) 100 N 3 Hz

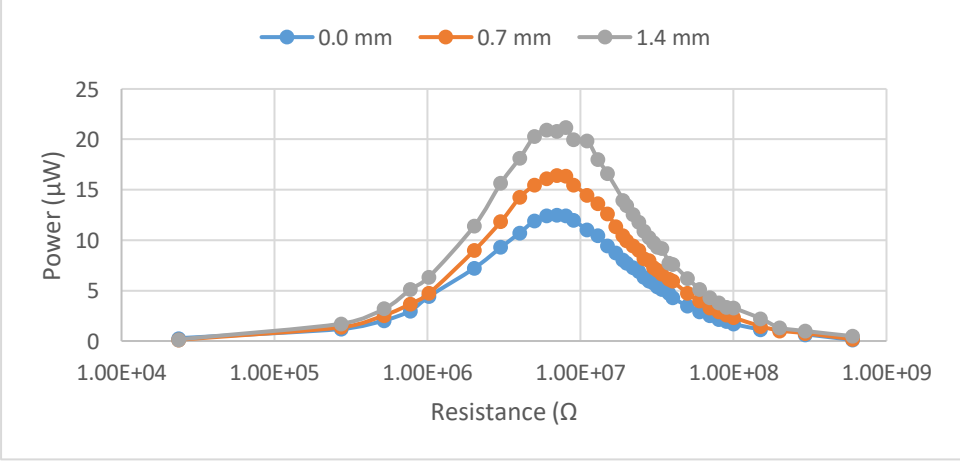

d) 100 N 5 Hz

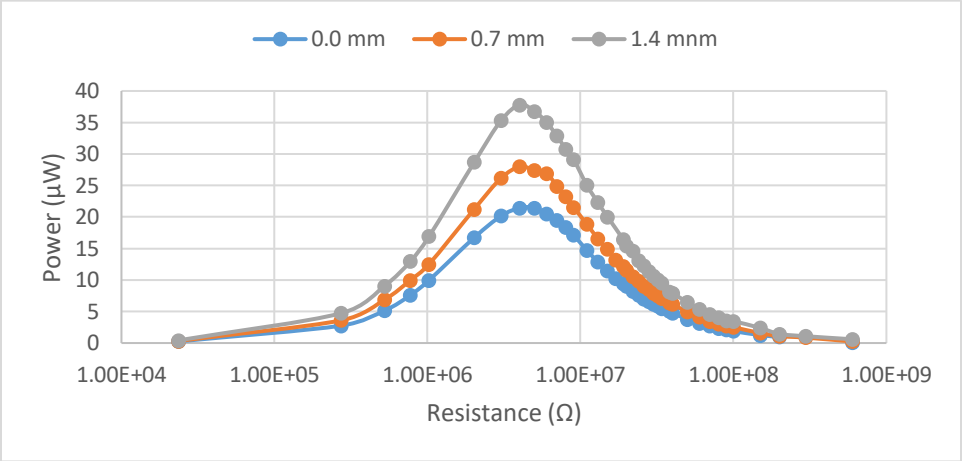

Figure 20. Average Power Across Resistance Sweep for 100 N and Varying Loading Frequencies. A) 100 N 1 Hz, B) 100 N 2 Hz, C) 100 N 3 Hz, D) 100 N 5 Hz

a) 500 N 1 Hz

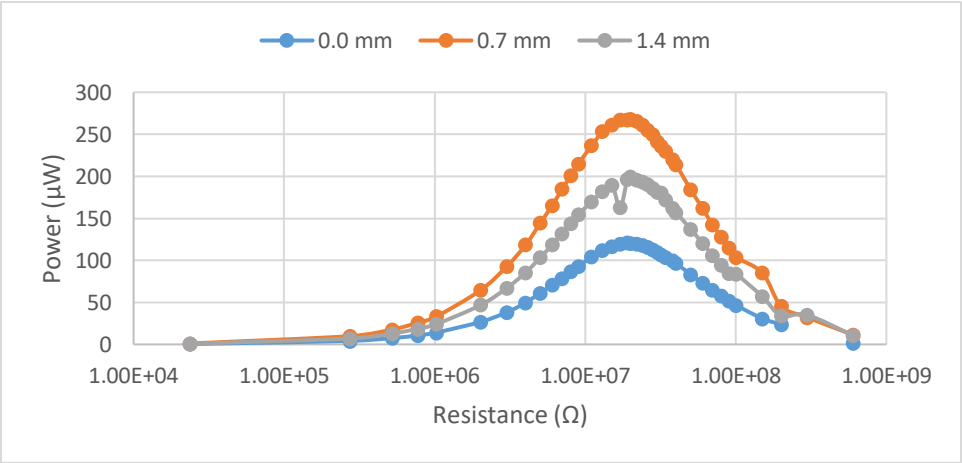

b) 500 N 2 Hz

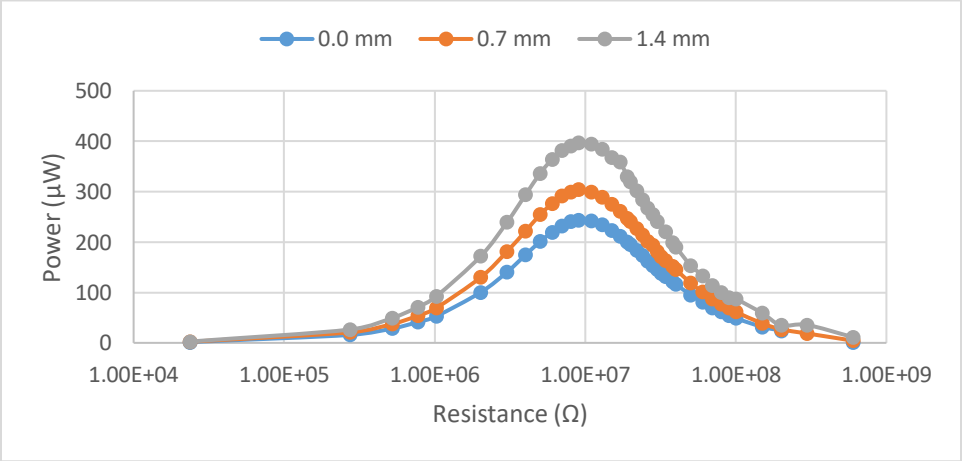

c) 500 N 3 Hz

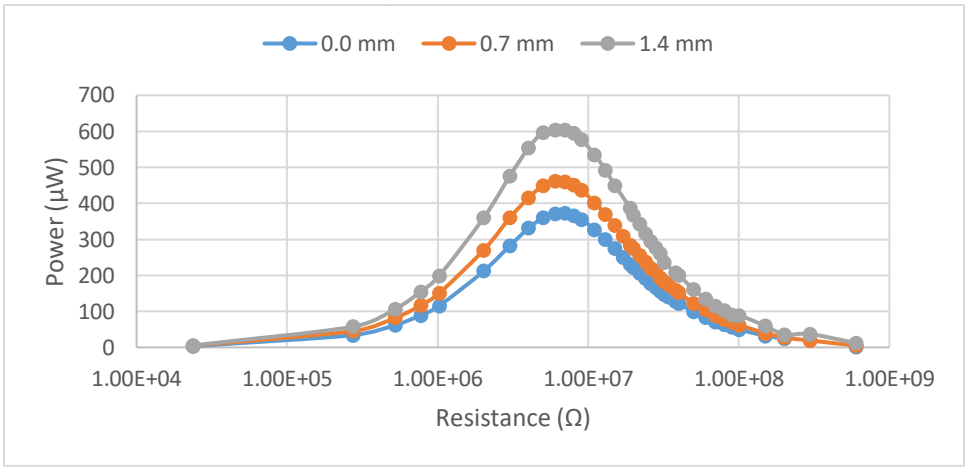

d) 500 N 5 Hz

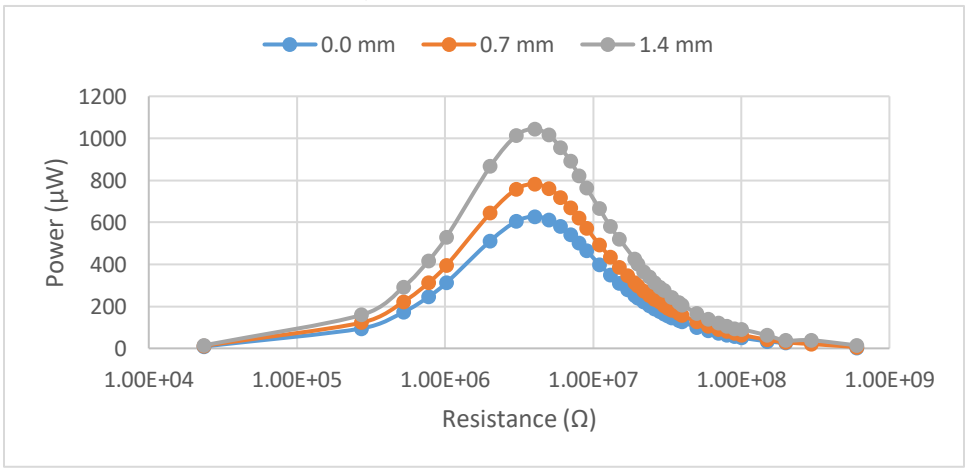

Figure 21. Average Power Across Resistance Sweep for 500 N and Varying Loading Frequencies. A) 500 N 1 Hz, B) 500 N 2 Hz, C) 500 N 3 Hz, D) 500 N 5 Hz

A) 1000 N 2 Hz

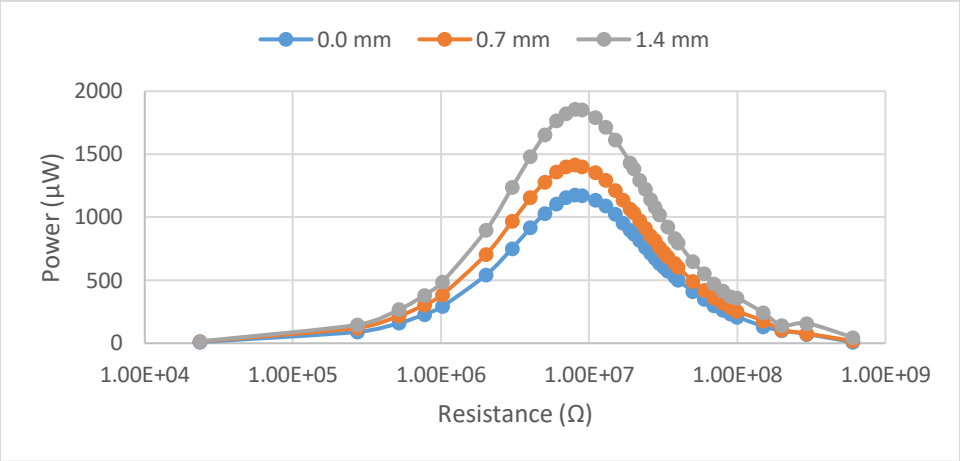

B) 1000 N 3 Hz

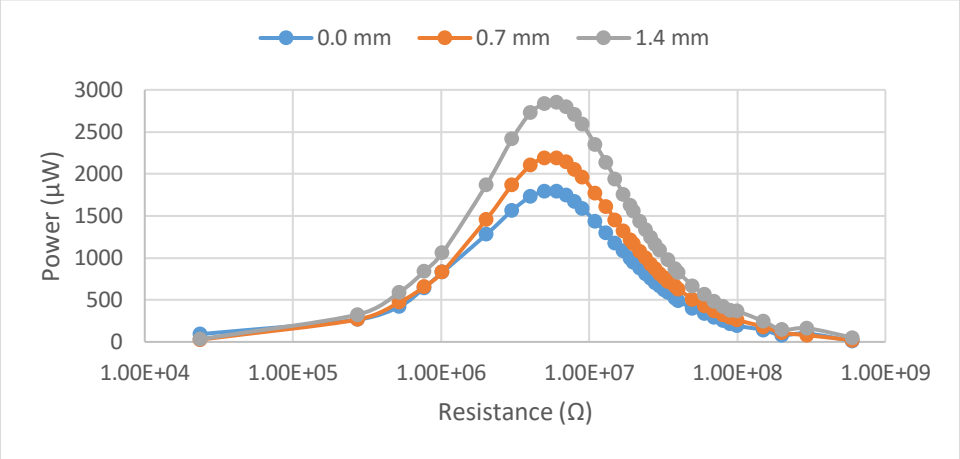

C) 1000 N 5 Hz

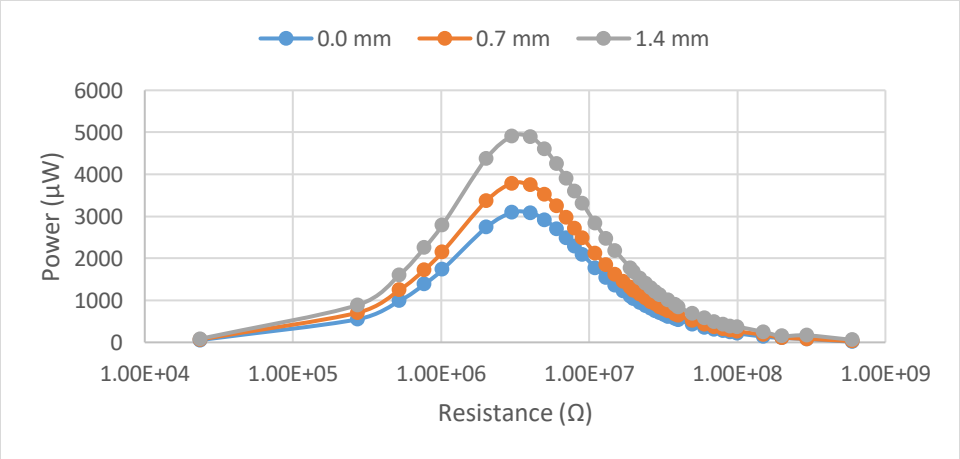

Figure 22. Average Power Across Resistance Sweep for 1000 N and Varying Loading Frequencies. A) 1000 N 2 Hz, B) 1000 N 3 Hz, C) 1000 N 5 Hz

D)

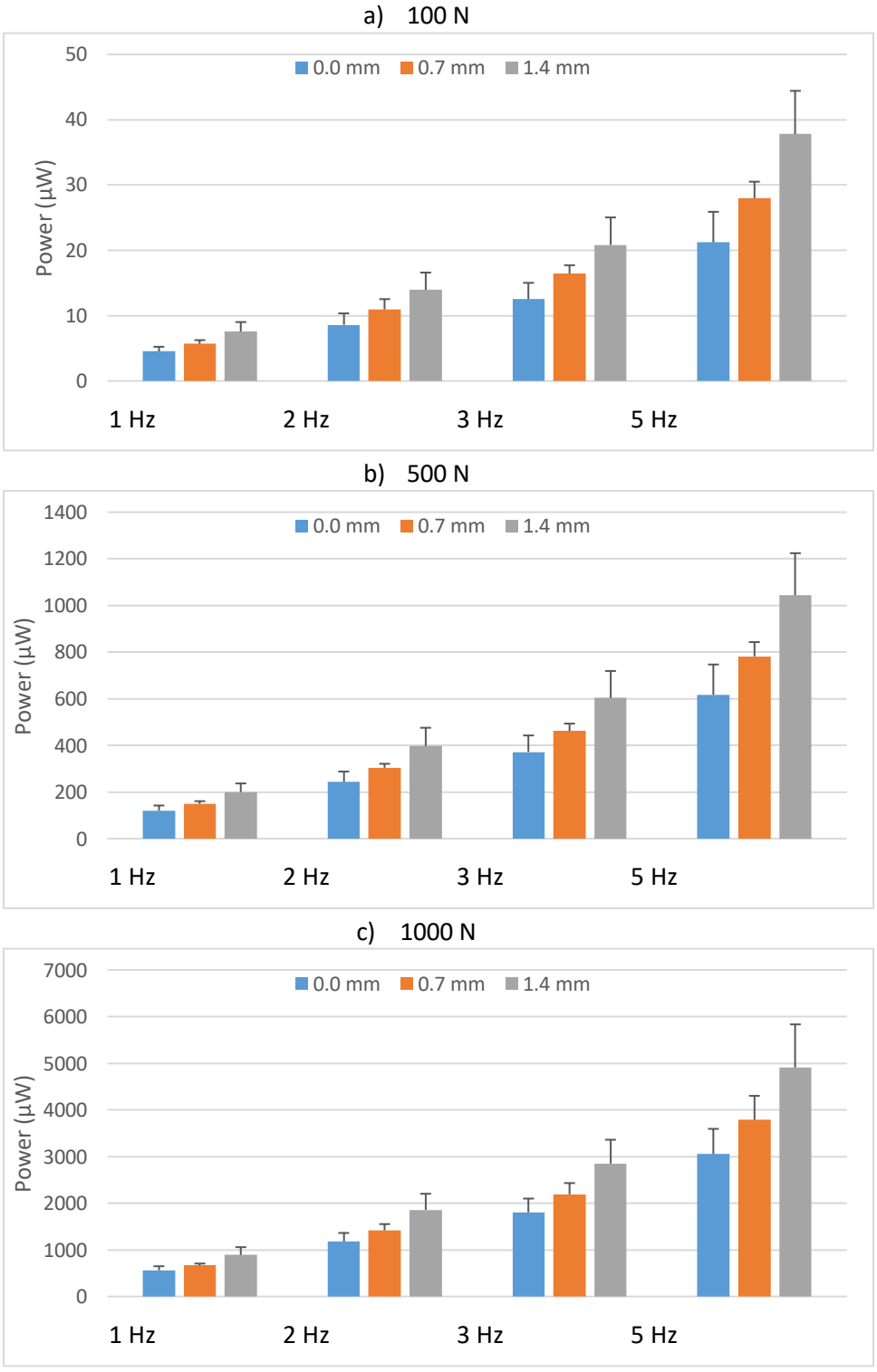

Figure 23. Average Power VS. Frequency
A) 100 N, B) 500 N, C)1000 N

a) 100 N

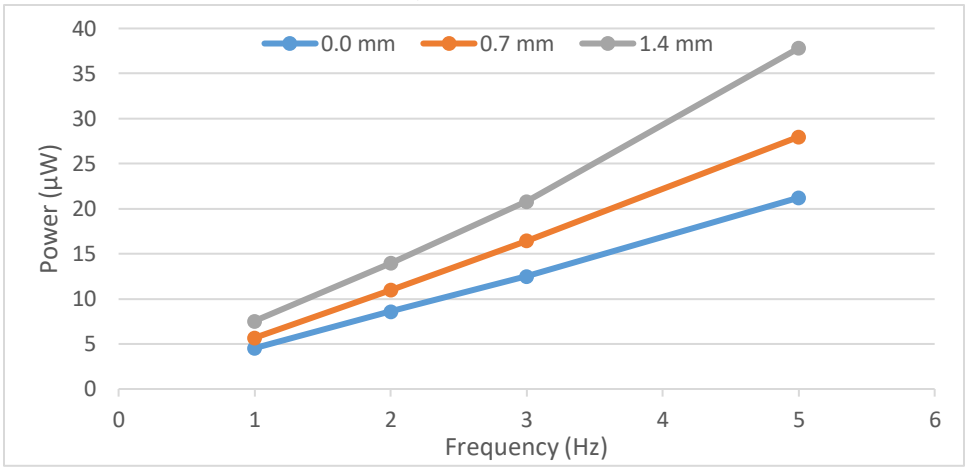

b) 500 N

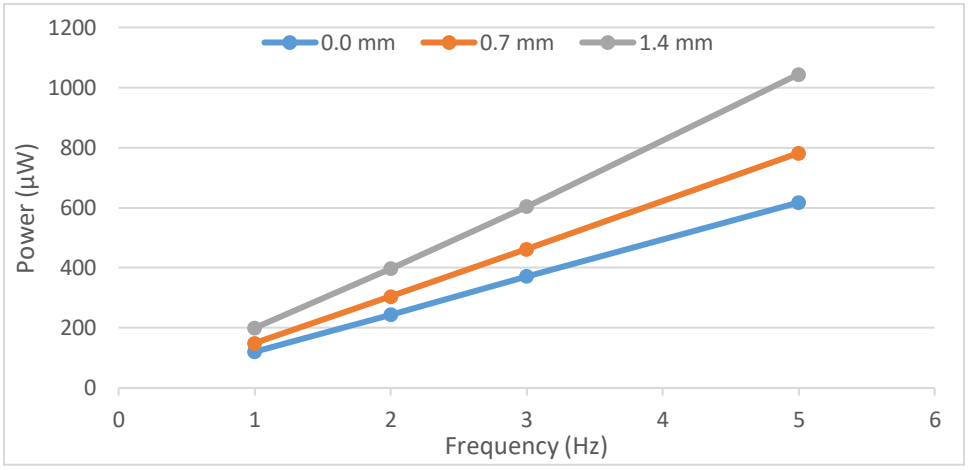

c) 1000N

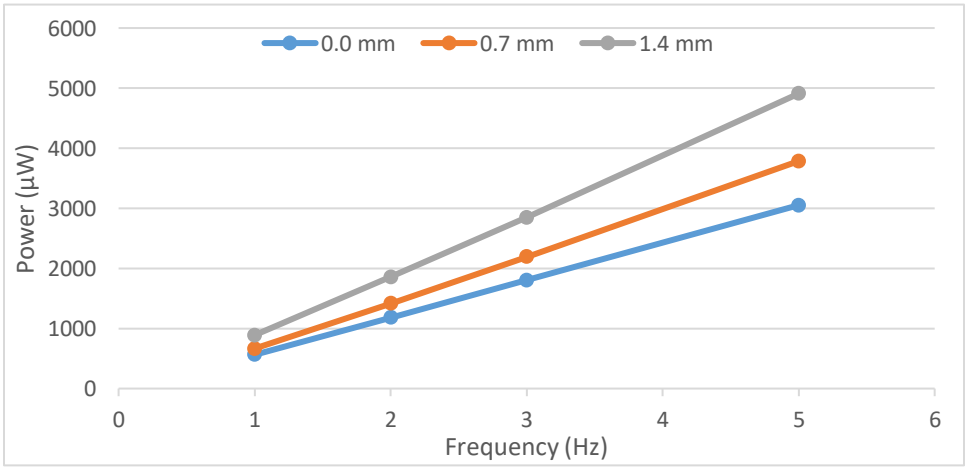

Figure 24. Average Power VS. Frequency A) 100 N, B) 500 N, C) 1000 N

Appendix B: Detailed Methods

Silicone Mold Fabrication

a. Create three aluminum cylinders of dimension 16 mm X 6.4 mm, 16 mm X 7.8 mm, and 16 mm X 9.2 mm for the 0T, 1T, and 2T specimen respectively
b. Create a small 5 sided box using small plexiglass pieces with a delron base adhering them with hot glue. It is imperative that a tight seal be made otherwise silicone will leak out
c. Make ~10g silicone using a 1:1 ratio of Part A:Part B
d. Place a single aluminum piece in the 5 sided box and pour silicone so that only half of the aluminum is covered. This will ensure that when the box is filled the aluminum piece will not float to the top.
e. Wait 2 hours for silicone to cure
f. Make another 10g, or as much to cover the aluminum piece completely, silicone using step C and pour into box and let cure for 2 hours
g. Remove cured silicone from box
h. Cut a slit in the silicone so that the aluminum can be removed
i. Label the silicone with the CL thickness of that mold
j. Repeat steps B through I for the other two CL thicknesses

Epoxy Mixing Method (5g yield)

a. Remove cover and turn on scale
b. Place plastic (never paper) cup on scale and zero scale
c. Using pipette add 4g of Part A
d. Using a different pipette (extremely important to use a different pipette) add 1g of Part B
e. Using a spatula mix Parts A and B together in a clockwise motion at 60 rpm for 50 cycles then again for 50 cycles in the anti-clockwise direction

Specimen Fabrication - Always wear surgical gloves when handling PZT

Determine if manufactured positive electrode was marked correctly.

a. Place PZT ring with manufactured marking up on a small piece of conductive material
b. Using a multi-meter on voltage lightly place the positive terminal on the marked electrode and the negative terminal on the conductive material
c. Using a short burst of air blow on the ring and observe the change in output voltage reading on the multi-meter
d. If the multi-meter shows a positive voltage the ring was correctly marked, if the multi-meter shows a negative voltage the side of the ring in contact with the conductive material is the positive electrode.

Wiring electrically in parallel same for all CL thicknesses

e. Remove conductive epoxy from freezer and allow to set in room temperature for 15 minutes
f. Align 3 rings with the positive side of each ring facing up on a flat sheet of delron
g. Cut 4 copper tabs (9 mm X 2 mm) and 2 copper tabs (30 mm X 2 mm)
h. Sharpen the wood end of a cotton swab

i. Using the wood end of the cotton swab apply a small amount of conductive epoxy to the top face of the ring in the pattern shown below

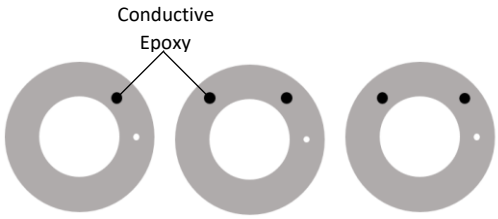

j. Using 2-9 mm copper tabs, place a tab to bridge from one epoxy dot to another as shown below

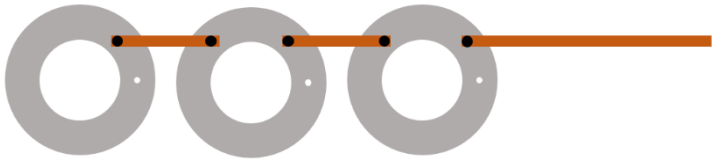

k. Place small amount of red silicone across each copper tab to stop conductive epoxy from curing to weight

l. Using 3 nuts, place them across the silicone to ensure conductive epoxy, copper tab, and PZT ring are adhered.

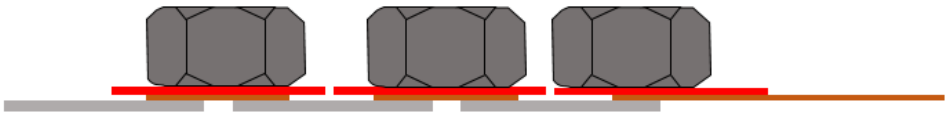

m. Turn oven on and set temp to 100°C
n. Place Delron sheet with copper tabbed rings in oven
o. After 1 hr remove using heat resistant gloves
p. Remove nuts and silicone and let cool for 10 minutes
q. Carefully flip the copper tabbed rings
r. Repeat steps d-l for the other side to resemble the figure below

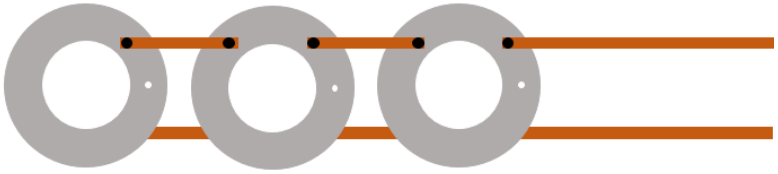

Encapsulation for (0.0 mm-0T CL)

s. Make a hallow cylinder of epoxy of dimensions 8.5 mm X 7.5 mm X 30 mm
t. Make a hallow cylinder of epoxy of dimensions 16 mm X 8.5 mm X 30 mm
    i. Steps O and P will be used for ensuring top, bottom, inner, and outer encapsulation thicknesses

u. Check connectivity by measuring the resistance across the stack with the multimeter set to measure resistance. If any resistance is measured determine where shorting occurred and fix shorting before proceeding.
v. Cut the cylinder made in step O into 6.5 mm sections
w. Cut the cylinder made in step P into 2 mm sections
    i. Before stacking is initiated, the two cylinders should be placed together resembling the image below. This will form the base for stacking and epoxy to adhere the PZT rings to

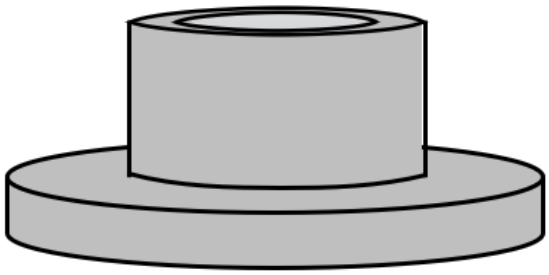

x. In an accordion fashion, ensuring the positive electrodes only touch the positive and the negative touch the negative, carefully fold the copper-tabbed rings.
y. Slide the stack over the base shown above
z. Using the wood end of a cotton swab, similar to that of the conductive epoxy, apply a small dab of epoxy to the spaces between the rings
aa. Place the top encapsulation ring on top of stack
bb. Place a red silicone slice on top of stack and place a nut on top of stack to apply compression to entire stack and let set for 24 hours
cc. After 24 hour, room temp cure, place in oven at 60°C for 2 hours
dd. After 2 hours remove from oven and let cool for 15 minutes then test connectivity by repeating step U
ee. Using the silicone mold previously made, pour a small amount of epoxy in the mold then insert the stacked specimen and continue to fill the mold till a small amount of epoxy comes out the top of the mold
    i. Before placing the specimen in the mold it should resemble the image below

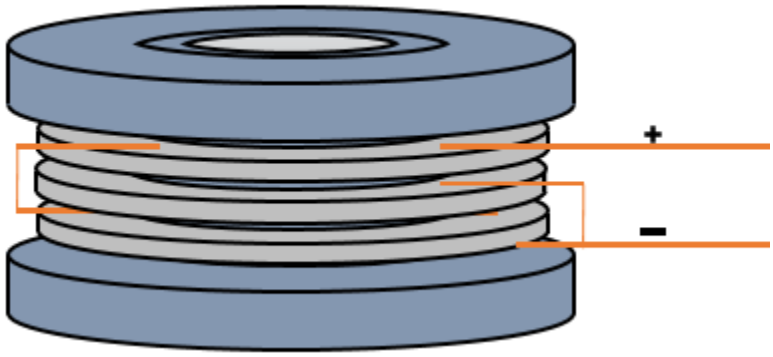

ff. Using two pieces of aluminum on either side of the mold parallel to the slot cut to insert the specimen, lightly clamp the mold until the slot in the mold is closed and let set for 24 hours

gg. Remove specimen from mold and place in oven at 60°C for 2 hours
hh. After 2 hours remove from oven and let cool for 15 minutes then test connectivity by repeating step U

Encapsulation for (0.7 and 1.4 mm-1T and 2T CL)

a. Make a hallow cylinder of epoxy of dimensions 8.5 mm X 7.5 mm X 30 mm
b. Make a hallow cylinder of epoxy of dimensions 16 mm X 8.5 mm X 30 mm
    i. Steps O and P will be used for ensuring top, bottom, inner, and outer encapsulation thicknesses
c. Make a hallow cylinder of epoxy of dimensions 14 mm X 8.5 mm X 30 mm
    a. This will be used for compliant layers
d. Check connectivity by measuring the resistance across the stack with the multimeter set to measure resistance. If any resistance is measured determine where shorting occurred and fix shorting before proceeding.
e. Cut the cylinder made in step A into 8 mm and 9.5 mm sections for 1T and 2T specimen respectively
f. Cut the cylinder made in step C into 0.7 mm and 1.4 mm sections
g. Cut the cylinder made in step B into 2 mm sections
    ii. Before stacking is initiated, the two cylinders should be placed together resembling the image below. This will form the base for stacking and epoxy to adhere the PZT rings to

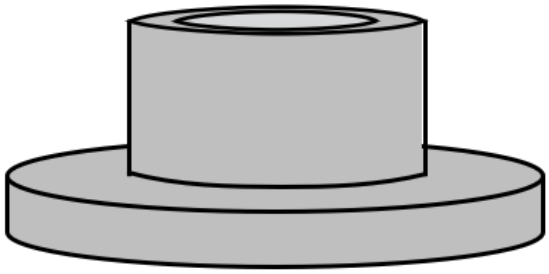

h. In an accordion fashion, ensuring the positive electrodes only touch the positive and the negative touch the negative, carefully fold the copper-tabbed rings.
i. Slide the stack over the base shown above
j. Using the wood end of a cotton swab, similar to that of the conductive epoxy, apply a small dab of epoxy to the spaces between the rings
k. Place the top encapsulation ring on top of stack
l. Place a red silicone slice on top of stack and place a nut on top of stack to apply compression to entire stack and let set for 24 hours
m. After 24 hour, room temp cure, place in oven at 60°C for 2 hours
n. After 2 hours remove from oven and let cool for 15 minutes then test connectivity by repeating step D
o. Using the silicone mold previously made, pour a small amount of epoxy in the mold then insert the stacked specimen and continue to fill the mold till a small amount of epoxy comes out the top of the mold

iii. Before placing the specimen in the mold it should resemble the image below

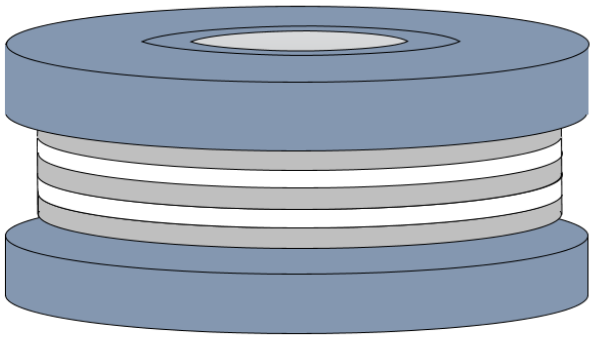

p. Using two pieces of aluminum on either side of the mold parallel to the slot cut to insert the specimen, lightly clamp the mold until the slot in the mold is closed and let set for 24 hours
q. Remove specimen from mold and place in oven at 60°C for 2 hours
r. After 2 hours remove from oven and let cool for 15 minutes then test connectivity by repeating step D

Appendix C: Data Processing Code

Main Stack Analysis MATLAB Code

```
%Data Analysis for Testing Piezoelectric Composites
%Originally written by John Doman in 2013
%Modified from code written by Ember Krech.
%Updated by Craig Cunningham December 2019

%Clear data
clear; close all; clc

%% Input Parameters

%Rmts = 2E6; %ohms %fixed MTS electrical resistance
Rmts = 23630; %ohms there is one 23.68 kohm resistor in parallel with MTS

%MAKE SURE TO DOUBLE CHECK THE RESISTANCE SWEEP VALUES!

numCatch = 0;
%% Load Desired Data
count = 1;
specimen_name = ['2T3_test_3']; %desired filename for analyzed data excel
file_location =
['D:\Research\Testing\2019_12_02_2T3_test3\']; %raw MTS data file location

output_file = ['Data ' specimen_name];
```

```
%Complete resistance sweep (37 resistances from .025Mohm to 600Mohm
Resistance_Sweep = [0 .25e6 0.5e6 0.75e6 1e6 2e6 3e6 4e6 5e6 6e6 7e6...
   8e6 9e6 11e6 13e6 15e6 17e6 19e6 20e6 22e6 24e6 26e6 28e6 30e6...
   32e6 34e6 38e6 40e6 50e6 60e6 70e6 80e6 90e6 100e6 150e6 200e6...
   296e6 602e6];

%number of loads used (100N, 500N, 1000N)
load = [1 2 3];

%number of frequencies used for each loading cycle (1Hz, 2Hz, 3Hz, 5Hz)
frequency = [1 2 3 5];

freqCount = 0;
for iFreq = 1:length(frequency)

   freqCount = freqCount +1;

   for iLoad = 1:length(load)

      for iResistor = 1:length(Resistance_Sweep)

%          iFreq = 1;   %You can change these to look at specific data
%          iLoad = 1;
%          iResistor = 1;

         name=[file_location 'specimen_xx_x_g33_PE_02_load_'...
           num2str(load(iLoad),'%.1d') '_' num2str(frequency(iFreq),...
           '%.2d') 'Hz_Rl_' num2str(iResistor,'%.2d.dat')];
         Reference_column(iLoad,iFreq,iResistor) =
         {['specimen_xx_x_g33_PE_02_load_' num2str(iLoad,'%.1d')...
           '_' num2str(iFreq,'%.2d') 'Hz_Rl_'...
           num2str(iResistor,'%.2d')]};

         dat = dlmread(name,'\t',5,0); %read in MTS data files

         Rvar = Resistance_Sweep(iResistor);

         %Store the data values into individual variables
         time = dat(:,1);
         axial_count = dat(:,2);
         axial_count = axial_count - min(axial_count) +1;
         x = -dat(:,3)*10^-3;   %m
         force = -dat(:,4);     %N
         voltage = dat(:,5);   %Volt

%          Plot raw voltage data
%          figure()
%          plot(voltage)
%          figure()
%          plot(force)
```

```
%% Filter the data to eliminate excess noise

%Calculate the sample frequency
deltaT = diff(time);
DeltaT = mean(deltaT);
fs = 1 / DeltaT;

%initial variables to use a low pass butterworth filter
fc =10 ; %Hz - cuttoff frequency

%filter data to eliminate excess noise. filter all data so
%that they are subject to the same phase delay
   [b,a] = butter(5,2*fc/fs);
   x  = filtfilt(b,a,x);
   F = filtfilt(b,a,force);
   Vmts = filtfilt (b,a,voltage);

   %Plot filtered voltage data

%           figure()
%           subplot(2,1,1), plot(voltage)
%           subplot(2,1,2), plot(Vmts)
%           ylim([min(voltage)+.001,max(voltage)+.001])
%           figure()
%           subplot(2,1,1), plot(force)
%           subplot(2,1,2), plot(F)

%Eliminate the initial and final portions of the data
%The MTS collects 15 cycles of each force, at each frequency,
%we only want to analyze the middle section (steady-state)

time = time(axial_count > 5 & axial_count < 27);
x = x(axial_count > 5 & axial_count < 27);
F = F(axial_count > 5 & axial_count < 27);
Vmts = Vmts(axial_count > 5 & axial_count < 27);
axial_count = axial_count(axial_count > 5 & axial_count < 27);

%       figure()
%       plot(Vmts)

%% Segment the data into 5 loading and unloading cycles
%This can be used to calcualte specimen stiffness, and d33/g33
%loading cycles
cycle1 = [10:2:18];

time = time(axial_count >= min(cycle1) &...
   axial_count <= max(cycle1));
x = x(axial_count >= min(cycle1) &...
   axial_count <= max(cycle1));
```

```
F = F(axial_count >= min(cycle1) &...
   axial_count <= max(cycle1));
Vmts = Vmts(axial_count >= min(cycle1) &...
   axial_count <= max(cycle1));
axial_count = axial_count(axial_count >= min(cycle1) &...
   axial_count <= max(cycle1));

timeL=time(find(ismember(axial_count,cycle1)));
xL=x(find(ismember(axial_count,cycle1)));
FL=F(find(ismember(axial_count,cycle1)));
VL=Vmts(find(ismember(axial_count,cycle1)));

timeU=time(find(ismember(axial_count,cycle1+1)));
xU=x(find(ismember(axial_count,cycle1+1)));
FU=F(find(ismember(axial_count,cycle1+1)));
VU=Vmts(find(ismember(axial_count,cycle1+1)));

%           figure()
%           plot(timeL, VL,'.')
%           hold on
%           plot(timeU, VU,'.r')
%           plot(time, Vmts,'g-')
%           figure()
%           plot(timeL, FL,'.')
%           hold on
%           plot(timeU, FU,'.r')
%           plot(time, Vmts,'g-')

%% Analyze Data

%Now the 5 middle cycles of filtered and phase corrected data
%This test was run in g33 setup, with a variable
%load resistance. The output voltage and power for each each
%resistance can now be analyzed

      Vmts = Vmts*(1/sqrt(2));%convert to RMS voltage
      Vout = Vmts.*(1+Rvar/Rmts);%scale voltage by the
                  %applied resistance to
                  %find voltage produced
                  %by the implant

      Vamp = (max(Vout) - (min(Vout)))/2; %calculate
                        %voltage
                        %amplitude
                        %peak-to-peak

      %instantaneous power
      P = Vout.^2./(Rvar+Rmts);
      %average power for all 5 cycles
      Pavg = trapz(time,P) * 1/(max(time) - min(time));
      %peak power per cycle
```

```
                Pmax = Vamp.^2./(Rvar+Rmts);
                %peak power per cycle in uW
                Pmaxu = Pmax*(10^6);

            %% Store data to output
            output(count,:) = {load(iLoad), [max(F)-min(F)],...
               frequency(iFreq), Rvar+Rmts, Vamp, Pavg, Pmax, Pmaxu};

            count = count + 1;

           %clear Vmts Vmts_shifted Rvar Vamp Pavg Pmax Vout Pmaxu
         end
      end
end

%% Output to an excel sheet for later analysis
output_header = {'Load' 'F-Range (N)' 'Frequency (Hz)'...
   'Resistance (ohm)' 'Voltage (V)' 'Pavg (W)' 'Pmax (W)' 'Pmax (uW)'};

output = [output_header; output];

   xlswrite([output_file '.xlsx'], output_header,1, 'A1')
   xlswrite([output_file '.xlsx'],...
      output(2:length(Resistance_Sweep)+1,:),'Sheet1','A2')

for ii = 2:12
   xlswrite([output_file '.xlsx'], output_header,ii, 'A1')
   xlswrite([output_file '.xlsx'], ...
      output((ii-1)*length(Resistance_Sweep)+...
      2:length(Resistance_Sweep)*ii+1,:),ii,'A2')
end

xlswrite([output_file '.xlsx'],output,13,'A1')

disp('Done')
```

```
%Data Analysis for Testing Implant in Femur Model
%Written by Craig Cunningham

clear; close all; clc;

%Defining Constants
implant_area=1.2252e-4;
implant_height=12/1000;
load=[0; 100; 250; 500; 750; 1000; 1250; 1500];
mload=[0; 100; 500; 750; 1000; 1250; 1500];
```

```
%Calculating Stress
mstress=(mload./implant_area)./(10^6);
stress=(load./implant_area)./(10^6);

%Inputing Strain Values
anterior=[0; 0; 24.67;43.33;13.67;-16.67;-43;-70];
lateral=[0;130.33;195.67;284.67;336.67;420; 498.67; 607.66];
posterior=[0;267.67;694.33;1650.67;2671;3595.33;4457.67;5279.67];
medial=[0; 654.33; 1469; 1854; 2179.67; 2510.33; 2868];

%%plotting the stress vs strain curve
plot(anterior,stress,'ro-')
hold on
plot(posterior,stress,'bs-')
plot(medial,mstress,'g+-')
plot(lateral,stress,'m*-')
xlabel(['Strain in uStrain'])
ylabel(['Stress in MPa'])
title(['Stress vs Strain'])
legend('Anterior Strain Gauge', 'Posterior Strain Gauge',...
   'Medial Strain Gauge', 'Lateral Strain Gauge','location','best')

%%calculating deformation for each strain gauge
del_a=0;
del_p=(posterior(8)*implant_height)/(10^6);
del_l=(lateral(8)*implant_height)/(10^6);
del_m=(medial(7)*implant_height)/(10^6);
```

Statistical Analysis SAS Code

```
*PZT Power Statistical Analysis
Written by Craig Cunningham;

* Clears the log;
dm 'log;clear';
* Clears the output;
dm 'output;clear;';

*Inputing Data;

DATA craig;
        INPUT load $ frequency $ CL $ power @@;
DATALINES;

A       I       n       4.140464868
B       I       n       110.0903551
C       I       n       522.2183106
A       II      n       8.331385479
B       II      n       219.7132497
C       II      n       1076.995011
```

A	III	n	12.56088971
B	III	n	339.0938081
C	III	n	1633.631469
A	V	n	21.10565415
B	V	n	572.8323291
C	V	n	2829.914247
A	I	o	6.04225578
B	I	o	155.5579989
C	I	o	684.9048583
A	II	o	11.84894112
B	II	o	316.3112927
C	II	o	1479.664304
A	III	o	17.62995218
B	III	o	478.6567949
C	III	o	2278.534796
A	V	o	30.8019154
B	V	o	819.4554867
C	V	o	3933.084822
A	I	t	7.161754804
B	I	t	175.5239172
C	I	t	836.0386242
A	II	t	11.45364587
B	II	t	345.7677776
C	II	t	1817.617671
A	III	t	17.48273448
B	III	t	518.7514752
C	III	t	2758.956657
A	V	t	35.1076029
B	V	t	941.9014216
C	V	t	4950.552803
A	I	n	5.538183349
B	I	n	150.9115521
C	I	n	678.1074022
A	II	n	11.10545894
B	II	n	305.0956787
C	II	n	1422.537811
A	III	n	15.79528053
B	III	n	465.8032561
C	III	n	2197.69626
A	V	n	27.40323936
B	V	n	788.7643847
C	V	n	3760.972548
A	I	o	5.549367474
B	I	o	150.0561117
C	I	o	624.208878
A	II	o	10.79718771
B	II	o	296.9089379
C	II	o	1268.126129
A	III	o	16.27172195
B	III	o	449.1961705
C	III	o	1938.382115
A	V	o	27.72249306
B	V	o	763.5456345

C	V	o	3227.915772
A	I	t	9.714506388
B	I	t	255.4501985
C	I	t	1134.536755
A	II	t	19.03777669
B	II	t	513.0322865
C	II	t	2336.113903
A	III	t	26.81205822
B	III	t	773.2022049
C	III	t	3560.622775
A	V	t	47.45122438
B	V	t	1311.972241
C	V	t	6115.891397
A	I	n	4.559669626
B	I	n	120.398294
C	I	n	570.5754484
A	II	n	8.029513269
B	II	n	246.0720124
C	II	n	1209.337801
A	III	n	11.98387299
B	III	n	372.4454354
C	III	n	1851.577233
A	V	n	20.31450324
B	V	n	627.9513417
C	V	n	3132.00836
A	I	o	4.83229825
B	I	o	133.041545
C	I	o	642.2529781
A	II	o	9.181382963
B	II	o	283.0779563
C	II	o	1344.128759
A	III	o	14.7225095
B	III	o	427.651622
C	III	o	2060.488758
A	V	o	24.69824608
B	V	o	704.4948387
C	V	o	3552.346582
A	I	t	6.787410618
B	I	t	185.1019637
C	I	t	832.440898
A	II	t	13.57457802
B	II	t	376.4910887
C	II	t	1757.111605
A	III	t	20.68706958
B	III	t	574.5735737
C	III	t	2731.048653
A	V	t	36.19398552
B	V	t	987.5717706
C	V	t	4688.747986
A	I	n	6.716211154
B	I	n	181.7522933
C	I	n	752.9351666
A	II	n	12.75150938

```
B	II	n	354.875224
C	II	n	1516.943827
A	III	n	18.33135186
B	III	n	549.8451648
C	III	n	2339.816913
A	V	n	32.4781515
B	V	n	935.3334323
C	V	n	3879.395549
A	I	o	6.359872555
B	I	o	159.0006116
C	I	o	711.927702
A	II	o	11.72486942
B	II	o	319.9068199
C	II	o	1571.143775
A	III	o	17.14316756
B	III	o	486.9826554
C	III	o	2483.777585
A	V	o	28.6862183
B	V	o	840.3562571
C	V	o	4427.829299
A	I	t	6.520917387
B	I	t	181.7522933
C	I	t	752.9351666
A	II	t	12.75150938
B	II	t	354.875224
C	II	t	1516.943827
A	III	t	18.33135186
B	III	t	549.8451648
C	III	t	2339.816913
A	V	t	32.4781515
B	V	t	935.3334323
C	V	t	3879.395549
;
RUN;
*Displays Data to Ensure Variables are Separated Correctly;

*PROC PRINT DATA=craig;
*RUN;

*Data Transformed to Assume Equal Variance;
data craig;
    set craig;
    logPOWER = log(power)/2;
  RUN;
*checking assumptions/requirements (START);
*running full 2way model, with interaction;
*this will allow a Normality test/plots, as well as an HOV plot (no test);
PROC GLM DATA=craig;
        CLASS load frequency CL ;
        MODEL logPOWER = load frequency CL  load*CL frequency*CL load*frequency load*frequency*CL;
        OUTPUT OUT=junk PREDICTED=yhat RESIDUAL=e;
QUIT;
PROC UNIVARIATE DATA=junk NORMAL PLOT;
```

```
        VAR e;
RUN;
PROC SGPLOT DATA=junk;
        SCATTER Y=e X=yhat;
RUN;
*Running one-way ANOVA to get BF test;
ODS SELECT HOVFTEST;

PROC GLM DATA=craig;
        CLASS load frequency CL;
        MODEL logPOWER = CL;
        MEANS CL / HOVTEST=BF;
QUIT;


PROC GLM DATA=craig;
        CLASS load frequency CL ;
        MODEL logPOWER = load frequency CL load*frequency load*CL;
QUIT;
*Comparing variables;
PROC GLM DATA=craig;
        CLASS load frequency CL;
        MODEL logPOWER = load frequency CL load*frequency load*CL;
        MEANS load frequency CL / HOVTEST=BF;
        OUTPUT OUT=junk PREDICTED=yhat RESIDUAL=e;
        LSMEANS load frequency CL / CL LINES PDIFF=ALL ADJUST=TUKEY ALPHA=0.1;
QUIT;
```